DISCLAIMER

This report was prepared as an account of work sponsored by an agency of the United States Government. Neither the United States Government nor any agency thereof, nor any of their employees, makes any warranty, express or implied, or assumes any legal liability or responsibility for the accuracy, completeness, or usefulness of any information, apparatus, product, or process disclosed, or represents that its use would not infringe privately owned rights. Reference herein to any specific commercial product, process, or service by trade name, trademark, manufacturer, or otherwise does not necessarily constitute or imply its endorsement, recommendation, or favoring by the United States Government or any agency thereof. The views and opinions of authors expressed herein do not necessarily state or reflect those of the United States Government or any agency thereof. Reference herein to any social initiative (including but not limited to Diversity, Equity, and Inclusion (DEI); Community Benefits Plans (CBP); Justice 40; etc.) is made by the Author independent of any current requirement by the United States Government and does not constitute or imply endorsement, recommendation, or support by the United States Government or any agency thereof.

Final Technical Report

Coal-derived graphene materials for industrial applications

December 29, 2025

Department of Energy (DOE)
Office of Fossil Energy (FE)
Award Number: DE-FE0032274

Principal Investigator
Patrick Johnson
Iowa State University

Co-Investigators
Trina Pfeiffer
Pilot coordinator, Pilot plant process development.
University of Wyoming

Dr. Kam Ng
University of Wyoming

Dr. Paul Behrens
Scale-up and TEA
University of Wyoming

EXECUTIVE SUMMARY

The project (Award DE-FE0032274), led by Iowa State University in collaboration with the University of Wyoming, sought to improve the production and utility of graphene oxide (GO), reduced graphene oxide (rGO), and related advanced materials from coal char. The three overall objectives of this project were: 1) to improve production of graphene oxide using Powder River Basin (PRB) coal as feedstock; 2) to continue testing and improvement of a hard carbon sodium-ion battery prototype and test device; and 3) to determine properties and performance of concrete using GO and rGO as a concrete additive or cement replacement.

This project demonstrated the conversion of Powder River Basin coal into valuable graphene-based materials, including graphene oxide, reduced graphene oxide, and hard carbon anodes for sodium-ion batteries. Major outcomes include: a reproducible flash pyrolysis process for high-carbon coal char; scalable synthesis of graphene oxide with high yields; production of quality reduced graphene oxide; incorporation of graphene oxide into concrete for up to 19% stronger compressive strength; and development of hard carbon anodes achieving high performance (277 mAh/g) and stability over 1000 cycles. These results confirm the feasibility of using coal-derived carbon for construction and energy storage, aligning with DOE goals for high-value coal products.

The technoeconomic evaluation performed under this project estimates the cost of graphene oxide derived from coal char to be $0.5/lb. This GO and rGO cost is orders of magnitude lower than commercially available materials, making this process a viable pathway for usage in a broad range of industries.

Table of Contents

INTRODUCTION

Background

The thermochemical process technology developed in the University of Wyoming School of Energy Resource's Center for Carbon Capture and Conversion (CCCC) efficiently decomposes Wyoming coal, yielding beneficial liquids and solids that are then used to create valuable, non-energy products, such as building and construction materials, asphalt products, and agricultural soil amendments. The core process technology integrates thermal coal solvent extraction and flash/thermal-pyrolysis processing and is a critical part of the overall carbon engineering program. CCCC researchers have worked with much success since 2016 refining the process and developing coal-derived carbon products. Wyoming has invested more than $30 million to date on such projects. The pyrolysis portion of the technology was installed to create larger volumes of coal char. The pyrolysis and related processes utilized in this project are shown in Figure 1.

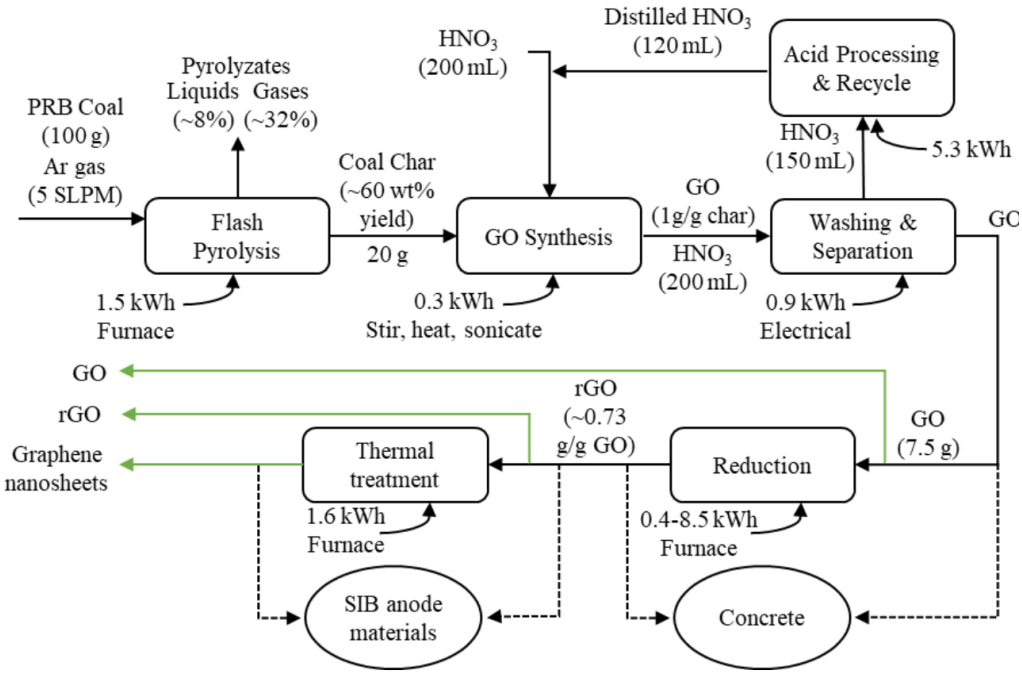

Figure 1. Block flow diagram of the overall production process and selected end use application.

Objectives

The main objective of this project is to further develop and demonstrate the feasibility of coal derived graphite oxide (GO), reduced graphite oxide (rGO), and graphene nanosheets with application to battery anode materials and cement filler. This work is designed to demonstrate the production process from coal feedstock to end-use products and show effectiveness of the anode material and concrete applications. The three overall objectives of this project are to improve production of GO using Powder River Basin coal as feedstock, conduct continued testing and improvement of a hard carbon sodium-ion battery prototype and test device, and determine the properties and performance of concrete using GO and rGO as concrete additive or cement replacement.

The main tasks of this study are designed to work towards applications for technologies that utilize domestic coal and/or carbonaceous coal residues to produce high-value graphitic products, through: (1) Flash pyrolysis of coal to obtain activated carbon; (2) optimization of the graphene oxide (GO) production process; (3) synthesis of reduced graphene oxide (rGO) and graphene nanosheets; (4) testing of GO and rGO as concrete additives/cement substitutes; (5) Fabrication and testing of hard carbon anodes in sodium-ion batteries (SIBs).

The success criteria were to obtain the final products in each of the steps according to the listed specifications: (1) Obtain coal char from instant pyrolysis of coal with a fixed carbon content of 68% and 80% devolatilization; (2) obtain GO from coal char with Raman D/G ratio higher than coal, and > 1; (3) obtain rGO with sharp (002) XRD peak and sp2/sp3 ratio of XPS > 3; (4) test concrete cylinders prepared with GO additive with minimum strength improvement of 10%. Successful products will be demonstrated through the development of coal char, GO, rGO and hard carbon anodes that offer properties that are superior to or unattainable with the current state of the art. 5) Battery criteria: reversible capacity of current density at 20 mA g^{-1} reach 266 mA g^{-1}, obtain 0.14 V or less as the ion extraction voltage, have the coulombic efficiency remain 80% after 15 cycles on the cycling stability test at 20 mA g^{-1}.

TECHNICAL APPROACH

Materials

Coal char

The pyrolysis process ensures a standard for the starting material (coal char) and consequent reproducibility in the synthesis of GO. This statement is based on the results presented in the flash pyrolysis process. As-received PRB coal was first crushed and sieved to 250-425 micron particles. The coal particles were fed through the pyrolysis reactor at 300-500 °C, with Argon as the carrier gas. The char produced was fed through the reactor again, from 700-1000 °C, with argon as the carrier gas. The initial pyrolysis step resulted in char devolatilized 38.4%, while the second flash pyrolysis step resulted in char devolatilized 81.1%. The coal char was delivered to the Materials Science and Engineering Department at Iowa State University for research on GO, rGO synthesis, high-efficiency batteries, Materials were sent back to UW to study their use as additive to cement / concrete. After receipt, the coal char is milled for 48 hours in a ball mill and used with a particle size of 120-150 micron particles. During the project a higher throughput flash pyrolysis system on the University of Wyoming campus was installed, enabling production of 5 kg of char per day ~10 kg of raw coal per day (summer 2024) and construction of a flash pyrolysis Semi Works plant in Gillette, WY with Wood Engineering is underway utilizing 6 tons per day (TPD) of raw coal feed.

Graphene oxide

Graphene oxide is produced using our nitric acid (HNO3) method. This method involves the oxidation of coal char in a nitric acid solution in a sonication bath for 4 hours, followed by filtration/washing until the solution reaches pH 3 and drying in an oven at 80 °C for 6 hours. This is a reliable and reproducible method capable of producing high-quality GO. However, a significant amount of waste (HNO3 solution) is also produced in large quantities. Reduced graphene oxide (rGO) is produced from the reduction of GO in a furnace at high temperatures (600 °C to 900 °C) in an inert atmosphere.

Cement and Aggregates
In this study, all concrete mixes were prepared using ordinary Portland cement conforming to ASTM C150/C150M-2233 specifications for type I/II. The specific surface area of cement was measured as 0.90 m2/g in accordance with ASTM C204-24.34 X-ray diffraction (XRD) analysis of the cement revealed its phase composition to be 8.16% dicalcium silicate (C_2S), 63.90% tricalcium silicate (C_3S), 5.79% tricalcium aluminate (C_3Al), and 10.37% tetracalcium aluminoferrite (C_4AF). The remaining are composed of secondary crystalline phases: gypsum dihydrate ($CaSO_4 \cdot 2H_2O$), gypsum hemihydrate ($CaSO_4 \cdot 0.5H_2O$), portlandite ($Ca(OH)_2$), titanium dioxide (TiO_2), magnesium oxide (MgO), sodium oxide (Na_2O), and potassium oxide (K_2O). Crushed granite with an angular shape was sourced locally from Laramie, Wyoming, and used as the coarse aggregate (CA), with a maximum aggregate size of 12.5 mm. The dry-rodded unit weight of the CA was determined to be 1590.73 kg/m^3, with an absorption capacity of 0.16% and a moisture content of 1%. The fine aggregate (FA), also locally sourced sand, had a fineness modulus of 2.58 and a rodded unit weight of 1586.68 kg/m^3.

Task 2. Flash Pyrolysis of Coal to Coal Char

Two different two-step processes were performed, both from as-received coal (12.5% moisture). The coal was "pre-pyrolyzed" at 500C, then one sample was flash pyrolyzed at 900C and the other at 1000C. The proximate analysis is detailed in Table 1 below, on a dry basis. The first row is the char after the pre-pyrolysis step.

Table 1: Pyrolysis temperature, volatile content wt%, fixed carbon wt%, and ash wt

Pyrolysis Temperature (°C)	Volatile Content wt%	Fixed Carbon wt%	Ash wt%
500	27.4	64.0	8.6
900	12.3	76.0	11.7
1000	8.6	79.8	11.6

A two-step process for char production was introduced in the last quarter in an effort to produce coal tar with lower concentrations of PAHs in the first, lower temperature mild pyrolysis step, and produce char with less volatiles after the second, high temperature flash pyrolysis step. As-received, PRB coal was first pyrolyzed at 500 °C in argon within the flash reactor. The char produced from this first step was then flash pyrolyzed in the same reactor at either 900 °C or 1000 °C, with Argon as the carrier gas. The first, "pre-pyrolysis" step resulted in char that was 37.4% devolatilized, while the second step resulted in char that was 72.0% and 80.4% devolatilized at 900 °C and 1000 °C, respectively. The volatile components of coal such as short and long chain hydrocarbons, aromatic hydrocarbons, water, sulfur species, and chlorine species were mostly removed. As listed in success criteria the values were obtained, ensuring the sequence of the synthesis and reduction steps of graphene oxide thought the coal char quality. The pyrolysis process ensures a standard for the starting material (coal char) and consequent reproducibility in the synthesis of GO. This statement is based on the results presented in the flash pyrolysis process. As-received PRB coal was first crushed and sieved to 250-425 micron particles. The coal particles were fed through the pyrolysis reactor at 300-500 °C, with Argon as the carrier gas. The char produced was fed through the reactor again, from 700-1000 °C, with Argon as the carrier gas. The initial pyrolysis step resulted in char devolatilized by 38.4%, while

the second flash pyrolysis step resulted in char devolatilized by 81.1%. Below is the proximate and ultimate analysis of the coal char.

Table 2: Proximate Analysis of Char from both Pyrolysis Steps

Pyrolysis Temperature (°C)	Volatile Content (dry wt%)	Fixed Carbon (dry wt%)	Ash (dry wt%)
300-500	27.0	64.2	8.8
700-1000	8.3	80.3	11.4

Table 3: Ultimate Analysis of Char from Flash Pyrolysis

Pyrolysis Temperature (°C)	% Carbon (Dry, Ash Free wt%)	% Hydrogen (Dry, Ash Free wt%)	% Nitrogen (Dry, Ash Free wt%)	% Oxygen/Sulfur (Dry, Ash Free wt%)
700-1000	89.8	1.2	1.4	7.6

The coal char was then delivered to the Materials Science and Engineering Department at Iowa State University for research on GO, rGO synthesis, high-efficiency batteries, and as an additive to Cement / Concrete. After receipt, the coal char is milled for 48 hours in a ball mill and used with a particle size of 120-150 microns.

Task 3. GO Process Optimization

Graphene Oxide production

A sonication bath and Schenck line enhanced the production capacity of graphene oxide in the laboratory up to 120 g per week. This improvement not only increases our ability to meet research demands but also opens doors for scaling up GO production for industrial applications. Figure 2 shows the increase in yield in mass percentage of the graphene oxide synthesis process from the modified nitric acid method.

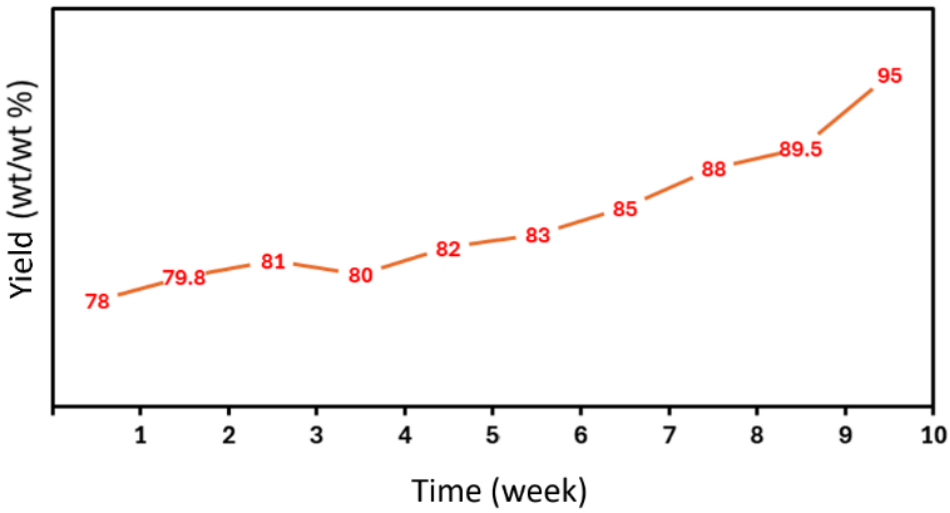

Figure 2: Yield in weight percentage for GO production.

The implementation of a Schenk line filtration, together with good practices in the synthesis process, enabled a higher processing speed from 120 g per week to 300 g. At the same time, there was an increase in the yield of the nitric acid oxidation reaction to obtain graphene oxide from 0.98 to 1.25, values relative to the precursor - 100 g of coal char yields 125 g of GO, see Figure 3a. The higher yields show that the oxidation rate of coal char has increased, that is, the amount of oxygen relative to GO is greater.

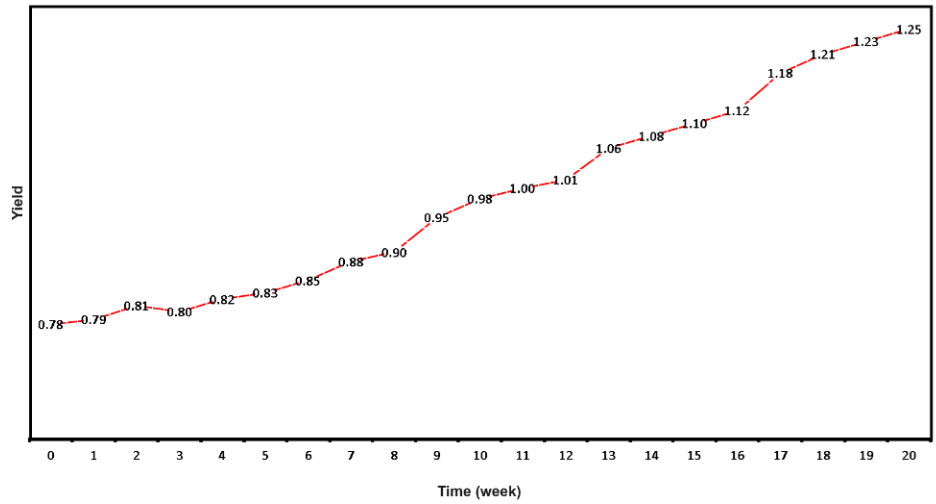

Figure 3a: Yield in weight percentage for GO production for the first 20 weeks.

Efforts to increase GO production were successful, and process changes were checked for consistency and scalability. Currently, obtaining GO from coal char using our method has only one filtration stage, making the process about three times faster. Longer sonication times allow for a reduction in the number of filtrations. By adopting 8 h of sonication, twice the time described in the method, it is possible to obtain GO with the same characteristics after one filtration. Extending sonication reduces the overall GO synthesis time because filtration is the most time-consuming step.

CHARACTERIZATION

Graphene Oxide

The feasibility of obtaining GO without filtration was studied, and the products were analyzed by X-ray diffraction and Raman spectroscopy, respectively Figures 3b and 3c. The diffractograms below display samples obtained from 1 and 4 filtrations (Filtrate 1 and Filtrate 4) and without filtration (HIT 1 and HIT 2), using direct heating to evaporate the nitric acid solution.

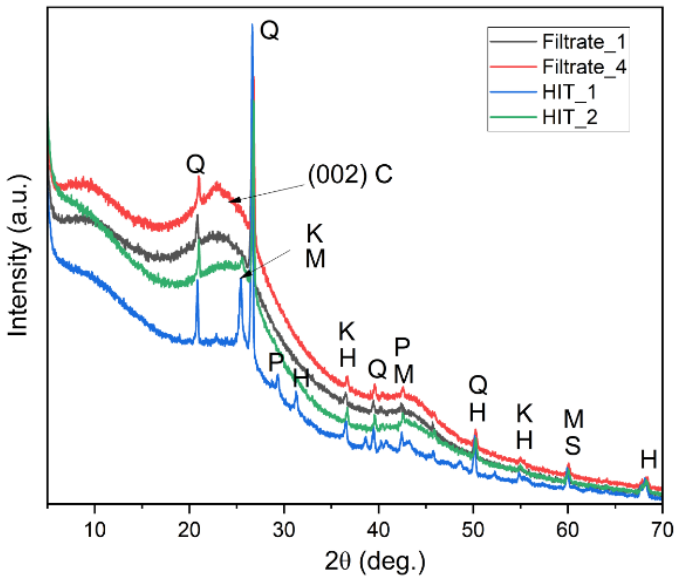

Figure 3b: XRD pattern for HIT1, HIT 2, filtrate1 and filtrate 4.

The major XRD patterns of coal char were quartz, kaolinite, mullite, and hematite or magnetite. One small peak was identified as pyrite. The HIT 1 sample peaks at 26.65°, corresponding to quartz reflection, indicating that this sample contains numerous sand particles. The peaks at 20˚-30˚ refer to the stacking structure of aromatic layers (graphite 002), and the broadening originated from the small dimensions of crystallites perpendicular to aromatic layers. This also indicates the few-layer graphene type of structure. HIT 2, Filtrate 1, and Filtrate 4 have broadened around 24˚ due to small dimensions of crystallites randomly oriented in different directions. Filtrate 1 and 4 exhibited peak broadening at 10˚, suggesting the presence of an oxygen functional group at the edges of the aromatic structure.

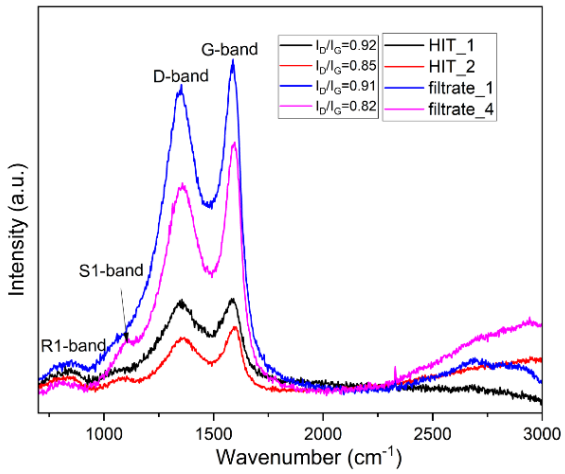

Figure 3c: Raman spectra for HIT 1, HIT 2, Filtrate 1, and Filtrate 4.

Carbon samples possess a characteristic G band peak around 1590 cm-1 and a D band peak at 1350 cm-1, representing the defect presence in samples. The peak around 800 cm-1 is attributed to C–C on alkanes and cyclic alkanes or C–H of aromatic rings (R1-band). The bump around 1060 cm-1 indicates mixed sp2–sp3 carbon hybridization (S1-band). HIT 1 possesses significant defects and a broad D band peak that might be due to quartz impurities. The filtrate 1 and filtrate 4 samples exhibit an intense G peak compared to the D peak, indicating sp^2 hybridized structures. Graphene oxide was produced from the pre-pyrolysis and pyrolysis of Powder River Basin (PRB) coal at 900˚ C and 1000 ˚C by our nitric acid method, process shown in Figure 4.

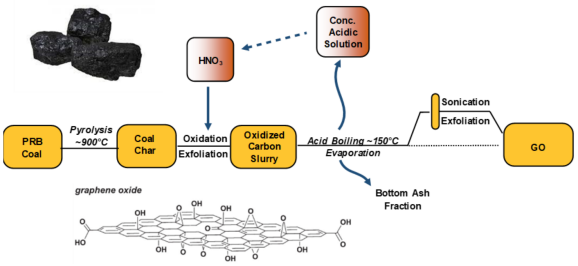

Figure 4: Scheme of the conversion of GO from raw coal to GO, and illustration of 2D chemical structure of GO.

As shown in Figure 5, we performed Raman measurements on the prepared GO samples and compared them with the Raman signals from coal char. All the samples show obvious D, and G peaks which are the Raman fingerprints of the carbon-based samples. We computed the area ratio of D to G peak (Indicated as D/G) for all of our measurements. As seen in Figure 5, the area ratios satisfy the criterion D/G > 1. Importantly, the D/G ratio of all three GO samples is larger than the coal char and improves successively with our filtration method optimization.

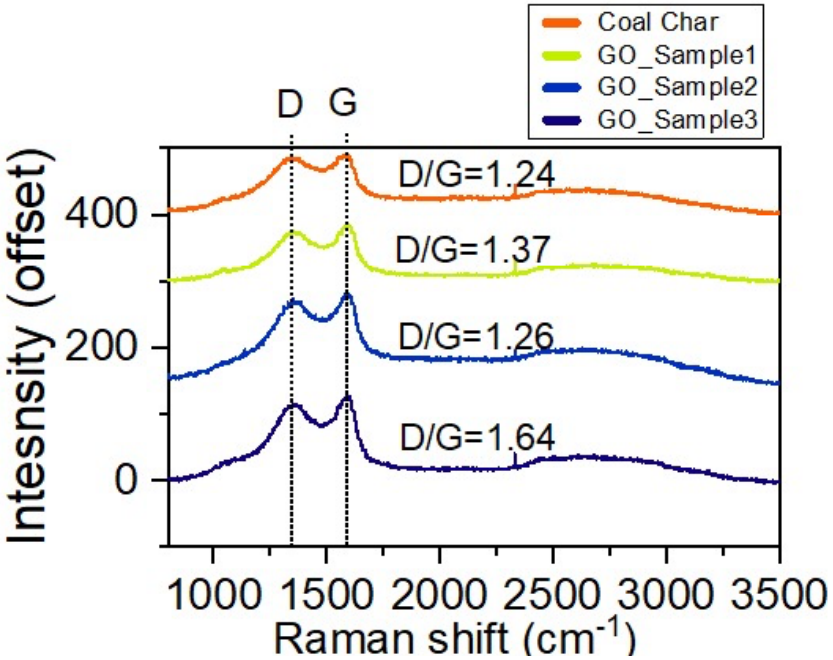

Figure 5: Raman spectrum to coal char and Graphene Oxide.

Further optimization may be needed to improve the process and improve the quality of the synthesized GO.

Reduced Graphene Oxide

In the next step, the prepared GO is heated to 1000 ºC for two hours in an inert atmosphere to make reduced oxide (rGO). The Raman analysis is shown in Figure 6 for the coal char, graphene oxide, and reduced Graphene Oxide.

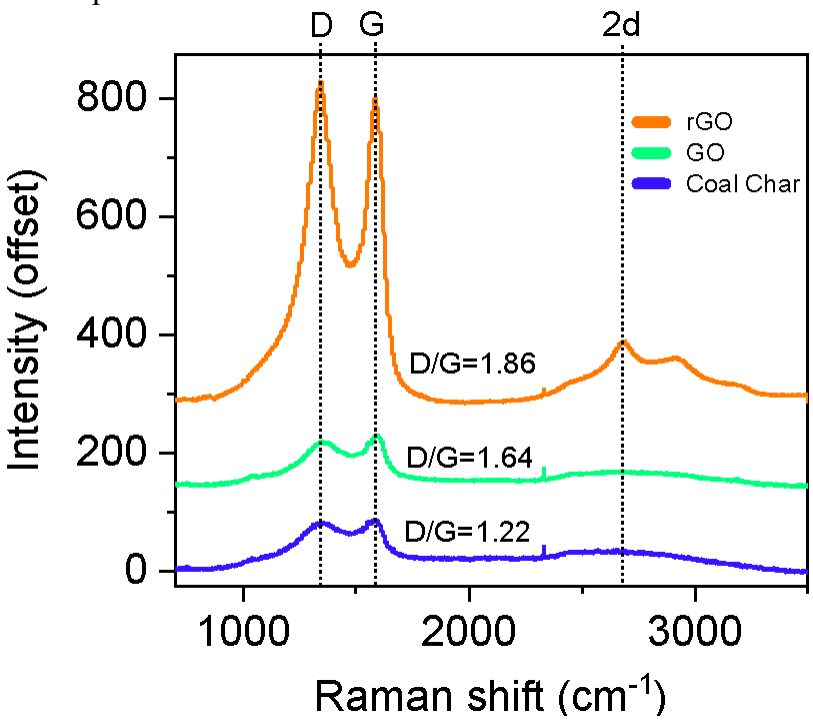

Figure 6: Raman spectrum of coal char, graphene oxide, and reduced graphene oxide.

The measurements from GO and coal char are shown for comparison. As can be seen from Figure 5, there is a continuous increase in D/G ratio during the successive steps. Interestingly, Raman spectra from rGO samples exhibited an additional 2D peak which is a signature peak of graphene-like materials.

One of the activities described in this project is to obtain GO from coal char and supply this GO to Kam Ng's group at the University of Wyoming for studies on the addition of GO to cement/concrete. The GO supplied was initially produced in batches of 20g and/or 40g, so it was important to ensure that all batches produced meet the same success criteria. Figure 4 shows the Raman spectra of different batches compared to the Raman spectrum of coal char and D/G ratios. The Raman analysis is shown in Figure 7 for the Graphene Oxide (1), Reduced Graphene Oxide (2), Coal char milled (3) and Coal char (4).

DE-FEO-0032274 – Final Technical Report

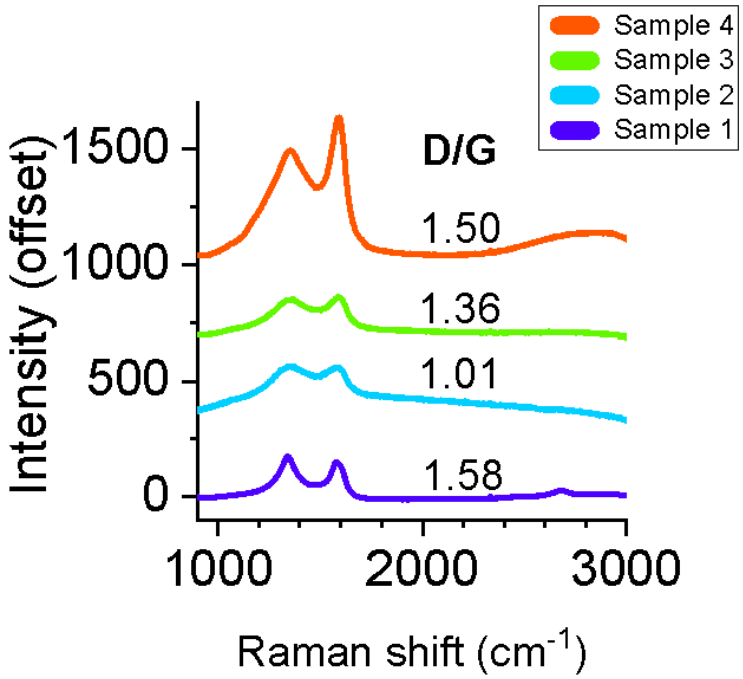

Figure 7: Raman measurements of the Graphene Oxide (1), Reduced Graphene Oxide (2), Coal char milled (3) and Coal char (4).

All samples show a clear G-band (at 1597 cm-1) a characteristic peak of the carbon materials, arising from in-plane stretching motion between sp2 carbon atoms. G-band peak is more intense in the coal char, which was not milled, indicating the more graphitic character of the sample. The presence of the D-band (1340 cm-1) indicates that all samples possess some degree of defects. The relative intensity ratio of D-band to G-band indicates the level of defects within the sample. The ID/IG ratio is higher in rGO than in GO because removing oxygen-containing functional groups left the defects in rGO. This is further indicated in the narrow 2D- band (at 2669 cm^{-1}).

rGO - sharp (002) XRD peak.
The primary results of FTIR show that from the coal char sample to the GO sample there is a significant decrease in the organic functionalities removed in the process of synthesizing GO. It is evident that after the GO was reduced, the species previously present were volatilized in the process. After confirmation of GO reduction, XRD analyses were performed, and the spectra are shown in Figure 8.

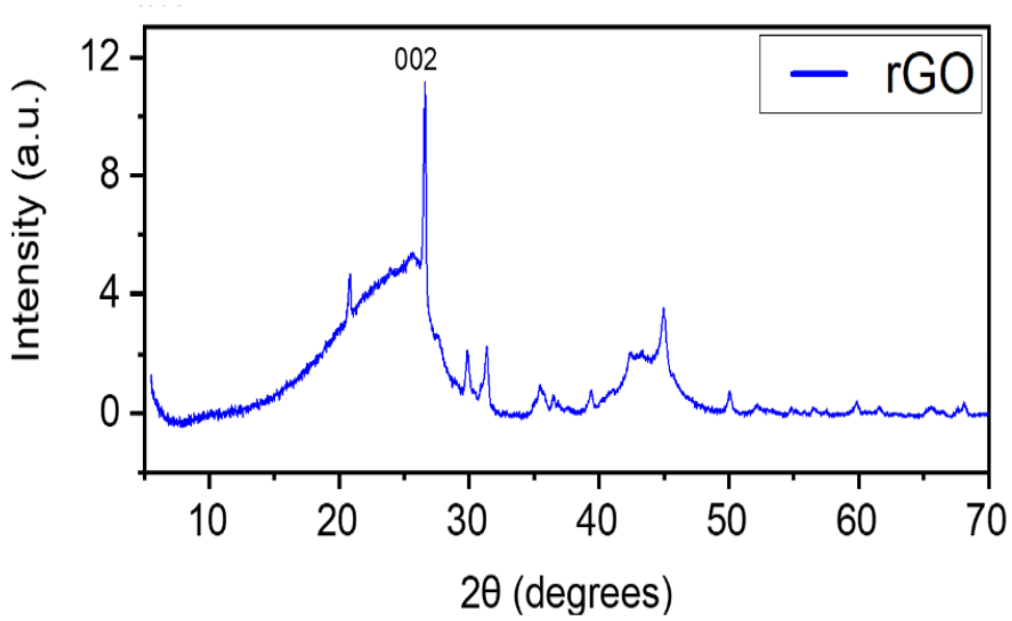

Figure 8: XRD spectra of coal rGO.

It is evident that the reduction of GO was effective due to the presence of the narrow peak at (002) 2 theta degrees at 26.5 for the rGO sample.

Task 4. Synthesis of rGO and graphene nanosheets

Obtaining Reduced Graphene Oxide (RGO) from Coal Char

Graphene oxide (GO) was synthesized using a modified nitric acid method, as previously reported. Among the available reduction techniques, chemical and thermal methods are the most widely used due to their simplicity, reliability, and high yield. Chemical reduction typically results in materials with higher electrical conductivity; however, it often introduces elemental impurities from the reductants into the GO structure. In contrast, thermal reduction at elevated temperatures yields a high carbon-to-oxygen (C/O) ratio and avoids the incorporation of impurities. In this study, we employed both reduction methods to achieve high conductivity and a favorable C/O ratio.

Chemical Reduction of GO

In the chemical reduction process, hydrazine hydrate was used as the reducing agent for GO. The X-ray diffraction (XRD) patterns are shown in Figure 9. Previous studies indicate that hydrazine hydrate preferentially removes -OH groups, followed by C=O groups, with C-O-C groups being the most resistant to reduction. Our results showed no significant reduction in either coal char GO, or biochar GO, suggesting that both materials contain a substantial amount of C-O-C groups, which are difficult to remove using chemical methods alone.

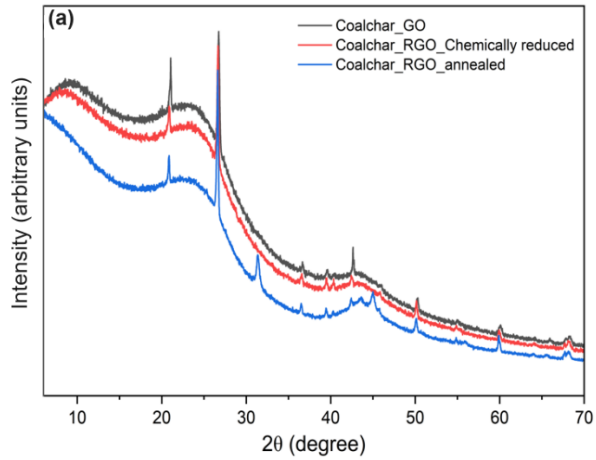

Figure 9: XRD spectra of coal char GO and the corresponding RGO sample.

Thermal Reduction via Annealing

We performed thermal reduction by annealing coal char GO at 800°C for one hour in a tube furnace to obtain RGO (Figure 10). The low-angle upturn in the background of the XRD spectra indicates the removal of oxygen-containing functional groups. The increased peak intensity after annealing suggests that the elimination of volatile components has strengthened the sp^2 bonding in the RGO structure.

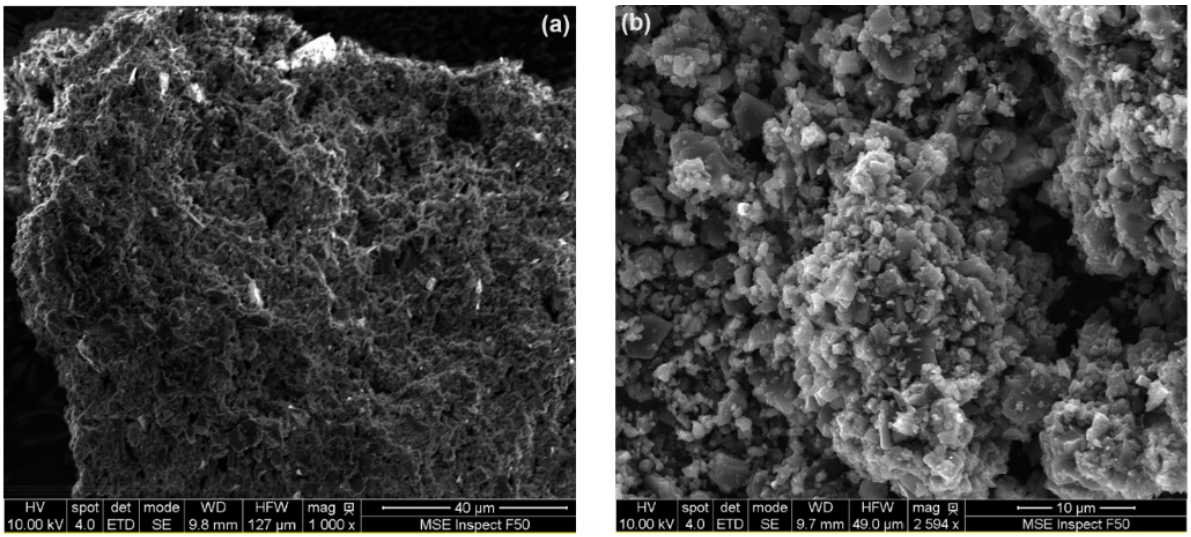

Figure 10: SEM images of (1) GO and (2) RGO after annealing.

The SEM images of GO and RGO, as shown in Figure 29, reveal a highly porous structure in the GO, where oxygen-containing functional groups are attached to the edges. After annealing, the removal of volatile substances such as CO_2 resulted in a reduction in particle size, further consolidating the RGO structure.

Raman analysis was performed using a Raman microscope with a 532 nm excitation laser. Figure 30 shows the Raman spectra of GO and RGO, both chemically reduced and annealed, for coal char samples. All samples exhibited the characteristic G-band peak at 1596 cm^{-1}, which

corresponds to the in-plane stretching vibrations of sp^2 carbon atoms. This G-band was particularly prominent in the coal char GO samples. No high-wavenumber peaks were observed in Figure 11 suggesting that the samples consisted of few-layer graphene.

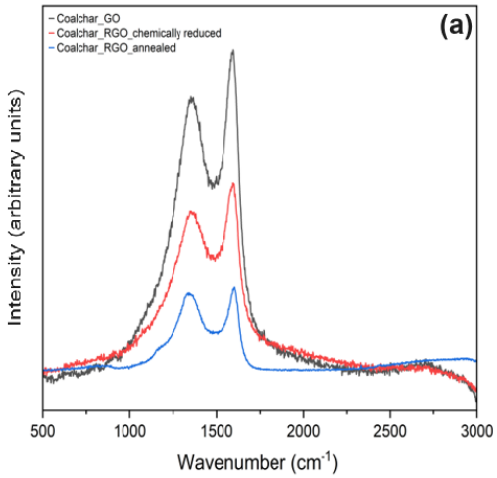

Figure 11: Raman spectra of coal char GO and rGO

For the chemically reduced rGO, the G-band intensity was lower, while the D-band, associated with the breathing modes of six-membered carbon rings, was more prominent in rGO. In annealed rGO samples, the D-band became dominant, indicating the removal of oxygen functionalities, which left vacancies and extended defects within the carbon matrix.

The nitric acid method used in graphene oxide synthesis generates significant waste, primarily in the form of acidic byproducts. The process involves strong oxidizing agents, such as nitric acid which can lead to the production of hazardous waste that requires careful disposal. Additionally, the reaction with carbon precursors often results in the formation of toxic gases, including nitrogen oxides (NOx).

Proper handling, neutralization, and disposal of these waste products are essential to minimize environmental impact and ensure compliance with safety regulations during the synthesis of graphene oxide. We successfully utilized waste nitric acid for the synthesis of rGO. Initially, coal char was treated with waste nitric acid, followed by the addition of a small amount of hydrogen peroxide at the final stage of the process. The samples were then filtered and dried. The X-ray diffraction (XRD) analysis, shown in Figure 12, reveals a broad peak at 25°, which confirms the formation of rGO.

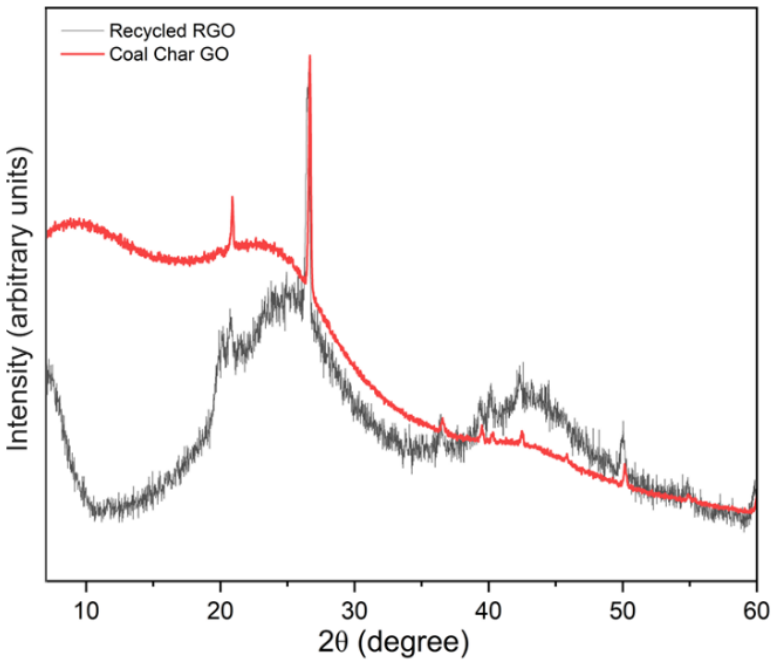

Figure 12: XRD spectrum to (a) coal char GO and recycled rGO

GO-assisted coal char hard carbon was prepared using 10% of GO with 90% of coal char. Figures 13 and 14 show SEM micrograph and Raman spectra of GO-assisted coal char.

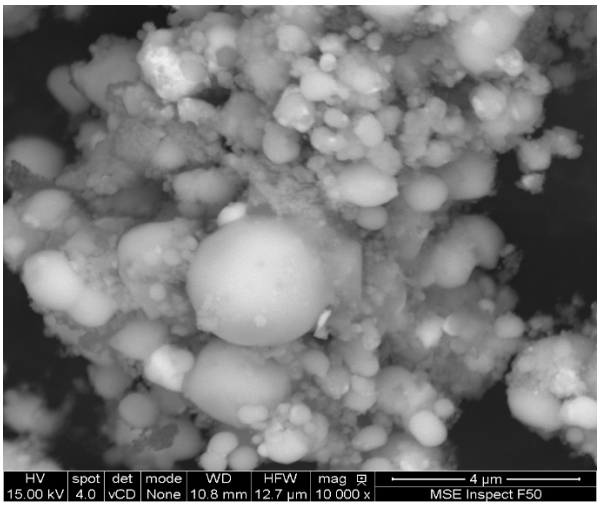

Figure 13: SEM images of GO/coal-char.

The GO/Coal-char showed a spherical morphology. Raman spectra revealed that GO/coal char possesses significant defects comparatively with GO derived from other sources.

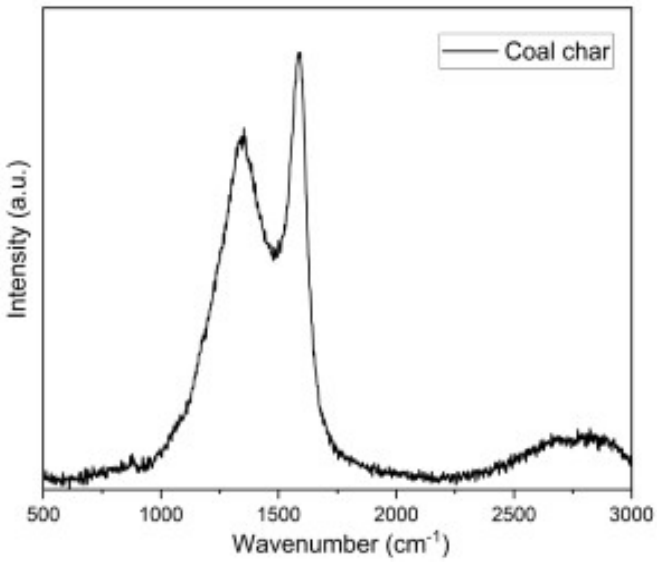

Figure 14: Raman of GO/coal char-derived hard carbon.

Task 5: Testing GO as concrete additive/cement replacement

The research group led by Professor Kam Ng at the University of Wyoming, and the Johnson research group at Iowa State University coordinated on Task 5 focusing on testing the performance of concrete with GO and rGO.

The Ng research group designed a concrete mixture incorporating the GO and rGO. The concrete design mix includes the characterization of coarse and fine aggregates and Portland cement, the determination of water to cement ratios, and the selection of fine to coarse aggregates ratios. Concrete molds, concrete mixer, pressing machine with axial and radial extensometers, a wet room for curing, a freeze-thaw chamber, and other equipment are prepared for this project. Concrete specimens without GO or rGO were prepared as the baseline for this project. The mechanical properties of baseline concrete specimens was then determined. The results have been significant, meeting the success criteria adopted for this part of the project.

All concrete samples in this study were prepared using Quikrete ordinary Portland cement Types I and II, following the specifications outlined in ASTM C150 [1]. In this study, a concrete mix targeting an unconfined compressive strength (UCS) of 30 MPa was designed based on a full characterization of the coarse and fine aggregates. This included assessments for gradation, specific gravity, unit weight, absorption, moisture content, and fineness modulus, all conducted in accordance with ASTM standards. Crushed angular granite stones and natural sand, both sourced from a local supplier in Laramie, Wyoming, USA, were used as coarse aggregate (CA) and fine aggregate (FA), respectively. The properties of the CA and FA are summarized in Table 4.

Table 4. Properties of CA and FA.

Property	Standard	CA	FA
Maximum Aggregate Size (mm)	ASTM C33 [2]	25.00	4.75
Minimum Aggregate Size (mm)		2.36	0.15
Bulk Specific Gravity (OD)		2.71	2.59
Bulk Specific Gravity (SSD)	ASTM C127 [3]	2.71	2.57
Apparent Specific Gravity		2.72	-
Dry rodded Unit Weight (kg/m3)	ASTM C29 [4]	1590.73	1586.68
Absorption Capacity (%)	ASTM C127 [3]	0.16	0.60
Moisture Content (%)	ASTM C566 [5]	1.00	3.20
Fineness Modulus (FM)	ASTM C136 [6]	7.78	2.58

OD-Oven-dried; SSD-Saturated surface dried.

Cylindrical concrete specimens with a diameter of 50 mm and a length of 100 mm were prepared for compressive strength tests following ASTM C39 [7] and for indirect split tensile strength tests according to ASTM C496 [8]. Concrete beam samples measuring 100 mm by 100 mm by 355 mm were also prepared for flexural strength tests as per ASTM C78 [9]. These specimens were cured for 3, 7, 14, 28, and 56 days for compressive strength testing, while split tensile and flexural strength tests were conducted on samples cured for 28 days. In the experimental setup, graphene oxide (GO) derived from coal char was incorporated into the concrete mixes in two scenarios: partial cement replacement and additive to concrete as shown in Tables 5 and 6.

Table 6 presents the concrete mix designs at a water-cement ratio of 0.6. In the sample ID notations, "D" denotes the project identifier, the number "6" refers to the water-cement ratio of 0.6, "G" indicates graphene oxide, and the following numbers represent the percentage of GO content (e.g., 5 refers to 0.05% GO). In the case of additives, the letter "a" is added to the percentage number to distinguish between replacement and additive scenarios.

Table 5. Mix design of concrete (by weight) with GO as a cement replacement.

Sample ID	GO percentage (%)	Water (kg/m^3)	Cement (kg/m^3)	GO (kg/m^3)	FA (kg/m^3)	CA (kg/m^3)
D6G0	0.00	228	380.00	0.00	876	788
D6G5	0.05	228	379.81	0.19	876	788
D6G10	0.10	228	379.62	0.38	876	788
D6G25	0.25	228	379.05	0.95	876	788
D6G50	0.50	228	378.10	1.90	876	788
D6G100	1.00	228	377.15	3.80	876	788
D6G200	2.00	228	376.20	7.6	876	788

Table 6. Mix design of concrete (by weight) with GO as a concrete additive.

Sample ID	GO percentage (%)	Water (kg/m^3)	Cement (kg/m^3)	GO (kg/m^3)	FA (kg/m^3)	CA (kg/m^3)
D6G5a	0.05	228	380	0.19	876	788
D6G10a	0.10	228	380	0.38	876	788
D6G25a	0.25	228	380	0.95	876	788
D6G50a	0.50	228	380	1.90	876	788
D6G100a	1.00	228	380	3.80	876	788
D6G200a	2.00	228	380	7.6	876	788

Fabrication Process and Testing

Aggregates were sieved and oven-dried for at least 24 hours before being incorporated into the concrete samples, adhering to ASTM C192 [10], and weight batching was done using a concrete mixer. Slump tests, following ASTM C143 [11], were conducted to measure consistency and workability. Cylindrical specimens were prepared and cured for up to 56 days, with mechanical testing using GCTS RTR-1500 triaxial equipment.

Stress-strain measurements from axial loading at a strain rate of 0.2% per minute were used to determine UCS and elastic properties, following ASTM C39 [7] for compression tests on specimens cured at 7, 14, 28, and 56 days. Flexural strength testing involved three rectangular concrete beams tested under 4-point loading circumstances, adhering to ASTM C78 standards [9] using an automatic Gilson AC-250MRF concrete compression machine. Using the same machine, indirect split tensile strength tests were done following ASTM C496 standards [8], with leather shims on the specimen's top and bottom.

Workability and Density of Concrete

Figure 15 presents the slump test results for concrete mixes incorporating varying percentages of GO, both for the cement replacement and concrete additive, under the D-W60 mix design (in this notation, "D" represents the project identifier, and "W60" indicates a water-cement ratio of 0.6.).

When GO is used as a replacement for cement (D-W60 Replacement), the slump values decrease significantly from 155 mm to 117 mm when GO increases from 0 to 0.25%, and the slump values decrease steadily thereafter at higher percentages of GO, highlighting the significant reduction in workability as a small GO content is utilized to replace cement. For the additive scenario (D-W60 Additive), where GO is used as an additive to the concrete mix, a similar trend of decreasing slump values is observed as GO content increases.

Both scenarios clearly reveal an inverse relationship between GO content and concrete workability. As the GO content increases, the reduction in slump at a higher percentage of GO indicates that it reduces the fluidity and workability of the concrete mix by absorbing water [12–14].

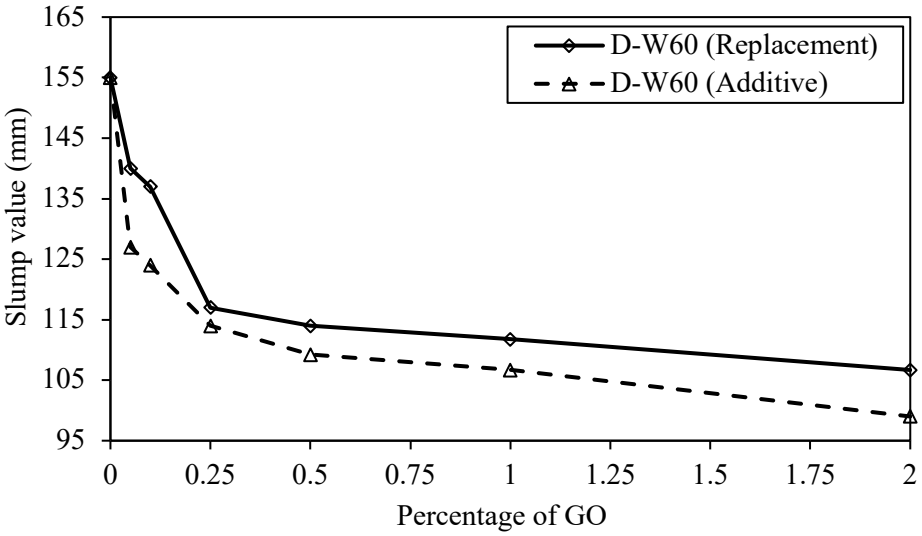

Figure 15. Slump test results of concrete mixes with different GO contents.

Figure 16 presents the density of concrete mixes with different GO contents. In both scenarios, it is evident that increasing GO content leads to higher concrete densities, due to a more compact and less porous concrete matrix contributed from GO. However, there are some slight variations in density trends between the replacement and additive scenarios, suggesting that the method of incorporating GO (as a replacement or additive) may affect the final microstructure and compaction of the concrete.

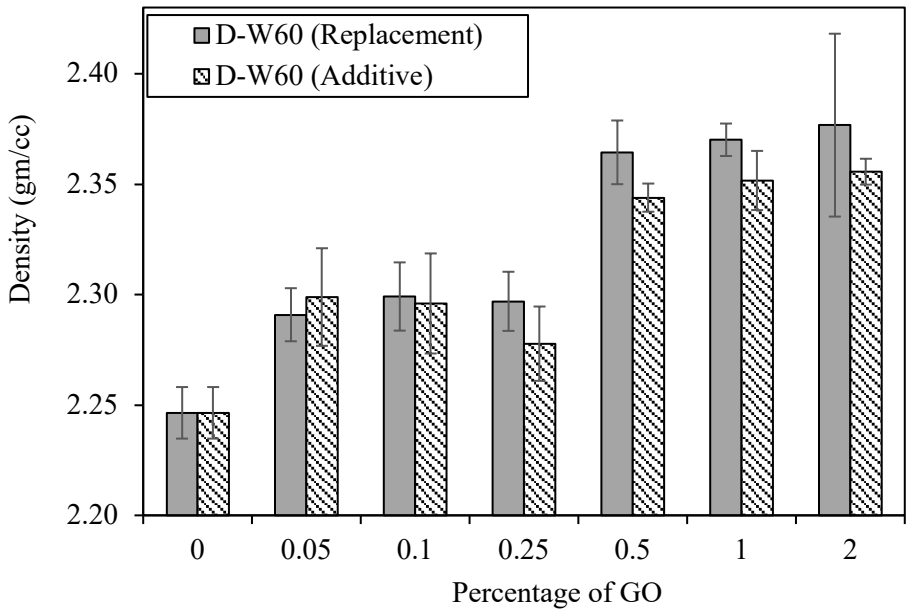

Figure 16. Density of concrete mixes with different GO contents.

Unconfined Compressive Strength of Concrete

Figure 17(a) presents the 28-day unconfined compressive strength (UCS) results for concrete mixes incorporating GO in both cement replacement and additive scenarios. Figure 36(b) presents the percentage increase in UCS with respect to the UCS of the baseline mix with 0% of GO. When GO is used as a cement replacement, the UCS increases with increasing GO content, reaching a maximum UCS of 35.2 MPa at 0.25% GO, or a 7.37% increase in UCS compared to the baseline mix. However, for GO contents between 0.5% and 2%, the UCS maintains at around 34.3 MPa, showing only minor variations at higher GO contents.

For the additive scenario, UCS enhancement is more pronounced. The UCS reaches its maximum of 37.5 MPa at 0.25% GO, a significant 14.4% increase in UCS. Although the UCS decreases slightly at higher GO contents, they are greater than the UCS 32.8 MPa of the baseline mix. These results indicate that GO is more effective as an additive in enhancing the concrete UCS than as a cement replacement. In both cases, 0.25% GO is the optimal content for strength improvement, with the additive scenario achieving the highest UCS. Exceeding this optimal content, the UCS values decline slightly, but additive mixes still outperform replacement mixes at higher GO contents.

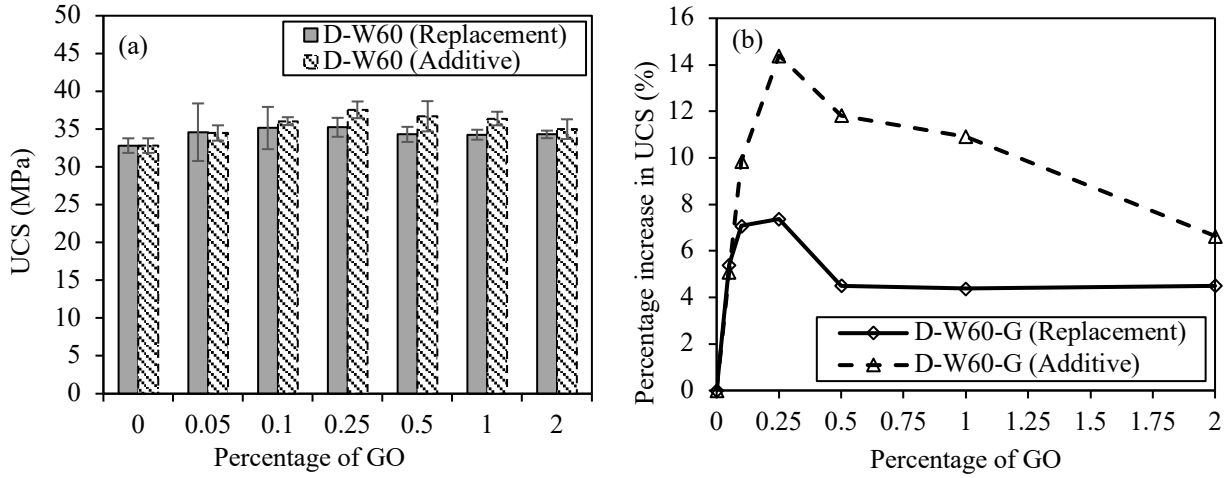

Figure 17. (a) Unconfined compressive strengths of concrete at 28 days of curing, and (b) percentage increase in unconfined compressive strength with respect to that of the control mix.

Flexure and Split Tensile Strengths of Concrete

Figure 18 (a) and (b) present the flexural and split tensile strength results for the concrete mixes, respectively. For the D-W60 (replacement) scenario, the flexural strength increases at a higher GO content, reaching a maximum flexural strength of 4.55 MPa at 0.5% GO. Exceeding this content, the flexural strength stabilizes to 4.24 MPa at 1% GO and 4.23 MPa at 2% GO. Similarly, the split tensile strength shows a similar pattern, with the highest value of 4.14 MPa at 1% GO and decreases slightly at both lower and higher GO contents. For the D-W60 (Additive) scenario, the flexural strength also increases with increasing GO content, achieving a maximum flexural strength of 4.5 MPa at 0.5% GO. The flexural strength increases slightly to 4.3 MPa at 1% and 2% GO.

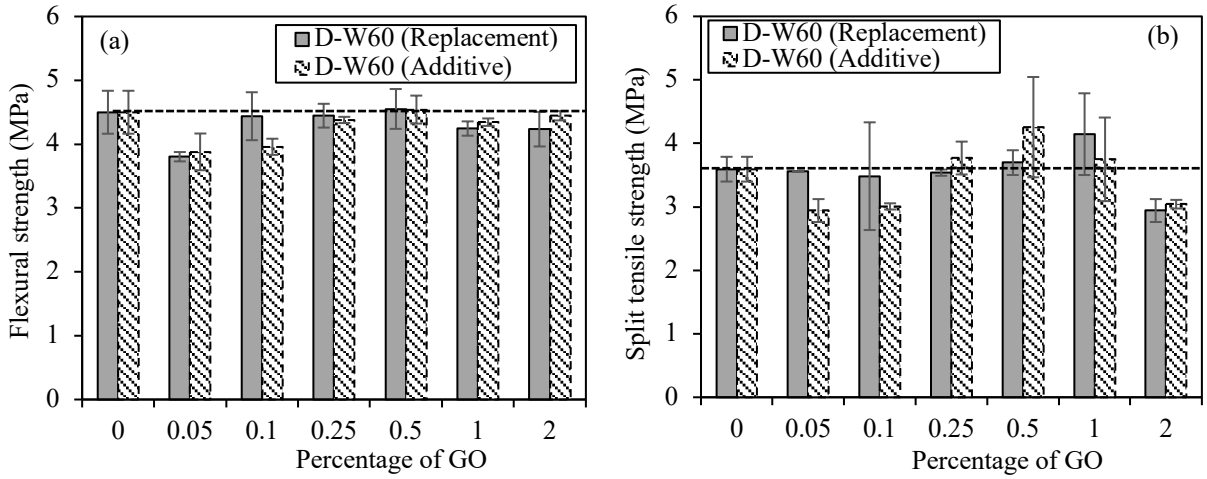

Figure 18: (a) Flexure strength and (b) split tensile strength of concrete at 28 days of curing.

The split tensile strength also follows an upward trend, reaching 4.26 MPa at 0.5% GO, indicating enhanced tensile strength with increasing GO content. Both the flexural and split tensile strengths exhibit positive trends as the GO content increases, with the additive scenario showing better performance than the replacement scenario, especially at higher GO contents. However, the flexural and tensile strengths of mixes at lower GO contents in both the replacement and additive scenarios are comparable to that of the baseline mix. This suggests the minimal impact of lower GO contents on flexural and tensile strengths.

Continued work focuses on evaluating the performance of concrete incorporating graphene oxide (GO) and reduced graphene oxide (rGO). Experimental works are being conducted to investigate the effect of GO on the engineering properties of concrete. The GO and rGO-modified concrete mix design has been developed for three different water-to-cement (w/c) ratios of 0.40, 0.50, and 0.60, with a constant fine-to-coarse aggregate (FA) ratio of 0.53. In the first phase, GO was introduced as both a partial replacement for cement and an additive in concrete at percentage levels of 0.05, 0.10, 0.25, 0.50, 1, and 2% by weight of cement.

Concrete specimens have been prepared and are undergoing controlled curing under-regulated humidity and temperature conditions in a wet room. Concrete specimens for the baseline and all GO percentages, both as a partial replacement and additive to concrete across varying w/c ratios, have been prepared to evaluate the key mechanical properties, including workability, density, compressive, tensile, flexural strength, and elastic parameters.

Tests were performed on another cement concentration, designated the D-W50 mix (in this notation, "D" represents the project identifier, "W50" indicates a water-cement ratio of 0.5) and the results shown in the figures below. The slump test of concrete with varying GO percentages is shown in Figure 19, under the D-W50 mix design. The graph shows a consistent decrease in workability as GO content increases from 0% to 2% in both replacement and additive scenarios. The highest slump is observed at 0% GO, while the lowest slump occurs at 2% GO. Replacement mixes exhibit slightly higher slump values than additive mixes at each GO level, though both follow the same declining trend.

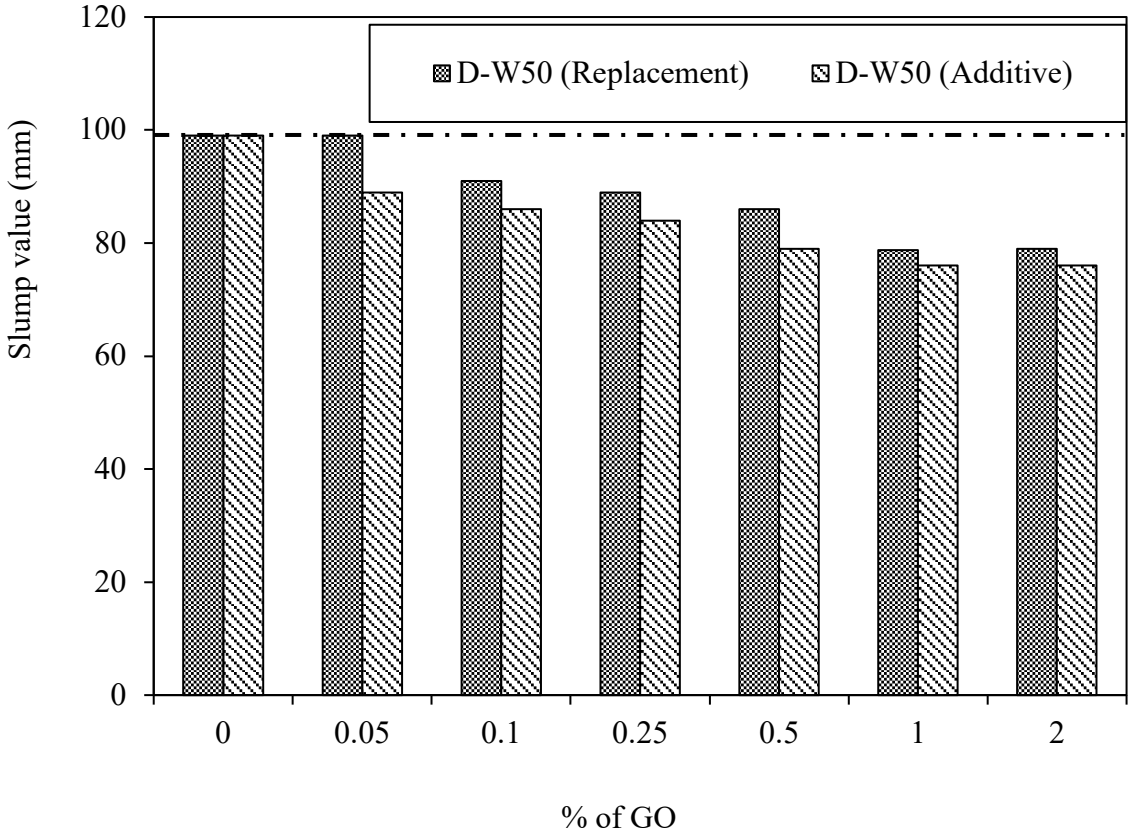

Figure 19. Slump test results of concrete mixes with different GO contents.

For density (Figure 20), increasing GO content from 0% to 2% results in higher concrete density in both scenarios.

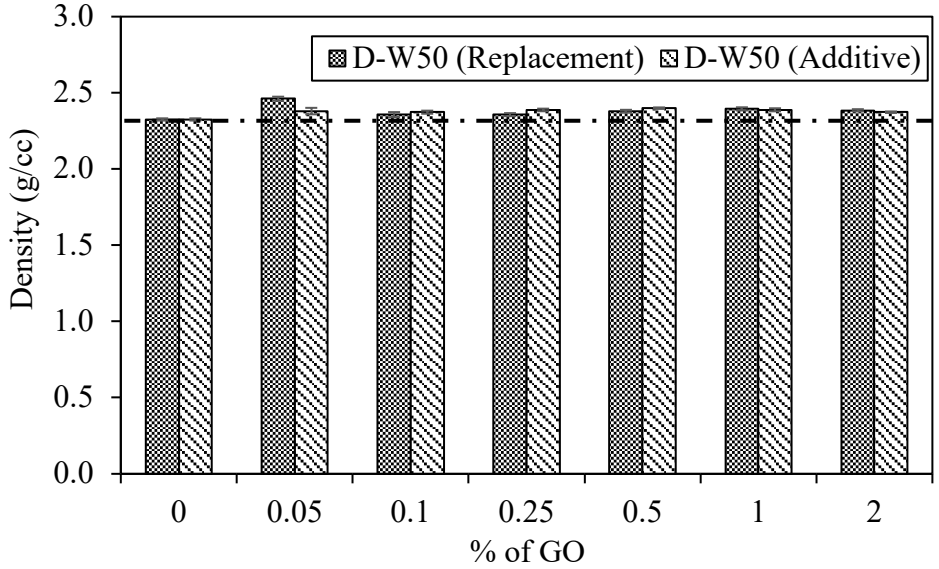

Figure 20. Density of concrete mixes with different GO contents.

Unconfined Compressive Strength of Concrete

The 56-day UCS results (Figure 21) demonstrate that strength improves with GO content up to 0.25% in both replacement and additive cases, peaking at the optimal range 0.10%. Beyond 0.25% GO, UCS values decline slightly but remain higher than the baseline (0% GO). The additive scenario consistently outperformed the replacement scenario, achieving the highest Unconfined Compressive Strength (UCS) at 0.10% Graphene Oxide (GO). Compared with the 0% GO, the UCS at 0.1% GO as an additive increased by 19%. The lowest strength is recorded at 0% GO, while the steepest drop occurs at 2%.

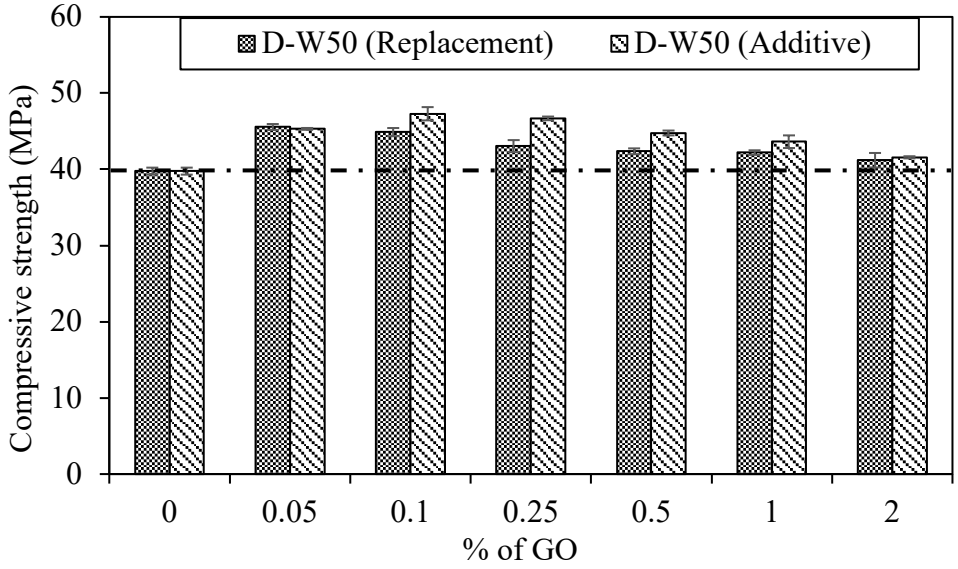

Figure 21. Unconfined compressive strengths of concrete at 56 days of curing.

Flexure and Split Tensile Strengths of Concrete

The flexural strength results (Figure 22) demonstrate improvement as GO content increases from 0% to the range of 0.10-0.25%, with the maximum 27% gain in flexural strength achieved at 0.1% GO for additive mixes. Beyond this optimal range, a gradual reduction in flexural strength is observed. The control mix (0% GO) exhibits the lowest flexural performance, while the replacement scenario shows comparable strength values to the additive mixes across most GO percentages.

A similar trend is evident in the split tensile strength results (Figure Rb), where tensile strength increases up to 0.05% GO for replacement mixes and 0.1% GO for additive mixes before experiencing a slight decline. The replacement mixes reach their maximum split tensile strength at 0.05% GO with a 20% gain. The additives mixes exhibit the maximum gain of 12% at 0.1% GO. Both test methods indicate that the optimal performance range for flexural and split tensile strength falls between 0.05% and 0.10% GO, with the replacement method showing particularly effective results in this range.

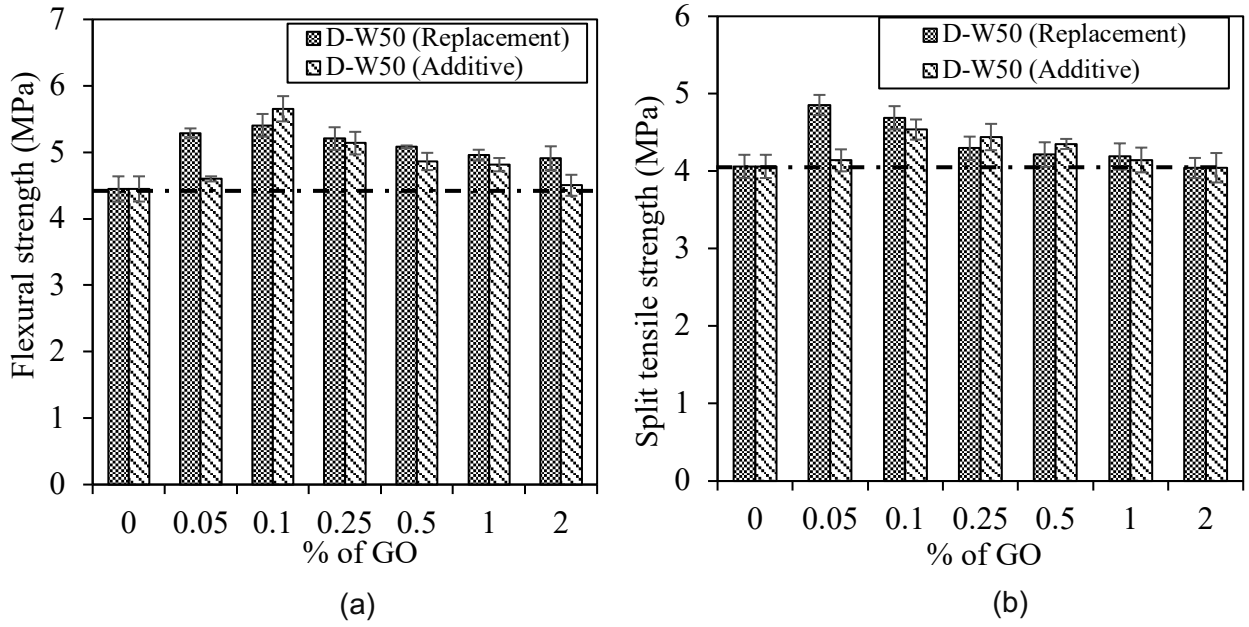

Figure 22. (a) Flexure strength and (b) split tensile strength of concrete at 28 days of curing.

Ng's research group (Wyoming) is making progress on Task 5, focusing on evaluating the performance of concrete incorporating graphene oxide (GO) and reduced graphene oxide (rGO). Researchers are studying how GO affects outcomes the engineering properties of concrete.

The mix design for GO and rGO-modified concrete has been developed for three different water-to-cement (w/c) ratios of 0.40, 0.50, and 0.60, with a constant fine-to-coarse aggregate (FA) ratio of 0.53. For the concrete mixes with GO, we have completed the analysis of all mechanical testing data, including compressive strength, flexural strength, tensile strength, density, modulus of elasticity, and Poisson's ratio. In addition, heat of hydration on concrete mixes with three water-to-cement (w/c) ratios (0.40, 0.50, and 0.60) has been conducted.

Task 6. Sodium ion battery fabrication/testing

Task 6.1: Using solvent extraction to produce ultra clean coal without mineral constitutes.

Developing high-performance hard carbon anodes for sodium-ion batteries is a critical focus of this study. Through a combination of chemical and thermal processing techniques, we aimed to optimize both the structural and electrochemical properties of hard carbon derived from coal char. The primary steps involved in achieving this goal included solvent extraction, oxidation, and thermal treatment to enhance the purity, interlayer spacing, and porosity of the hard carbon material. The presence of mineral impurities in coal presents significant challenges for its utilization in various applications, particularly in energy production and the fabrication of advanced carbon materials. Traditional methods of coal cleaning often leave trace minerals that can negatively impact performance and environmental sustainability. Solvent extraction has emerged as a promising technique to address these issues by effectively removing mineral constituents from coal. In this study, N-Methyl-2-pyrrolidone (NMP) was employed as the solvent

for extracting coal char, with the extraction at 200°C under an inert argon atmosphere. The treated coal was centrifuged and filtered, yielding an ultra-clean coal product. X-ray diffraction (XRD) analysis of the hard carbon derived from the extracted coal showed no detectable mineral peaks, providing evidence of a highly efficient mineral removal, Figure 23. This technique offers a pathway to producing high-purity coal, suitable for applications requiring minimal mineral content.

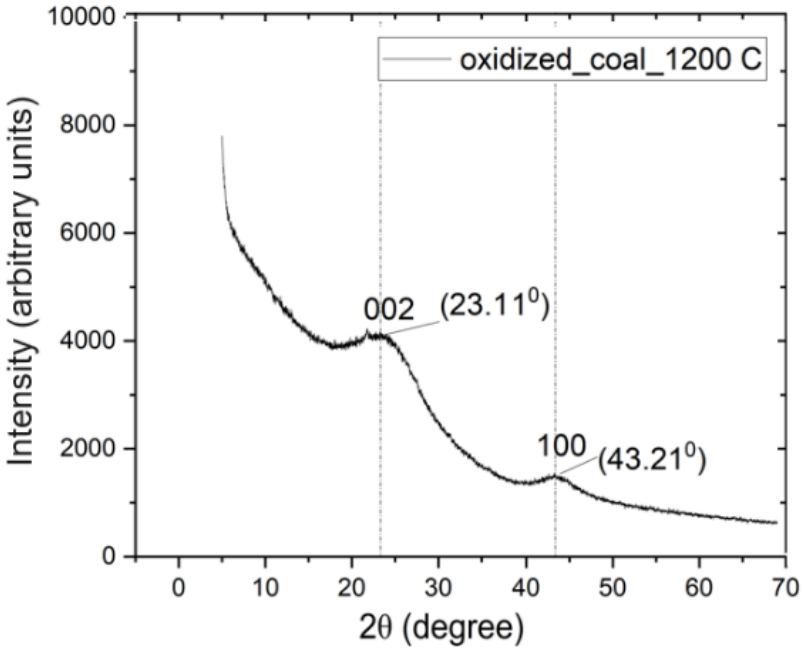

Figure 23: Oxidized coal char annealed at 1200 °C.

Task 6.2: Oxidizing extracted coal using nitric acid as a strategy to increase the interlayer spacing of annealed hard carbon anode battery.

Optimizing interlayer spacing in hard carbon is critical for enhancing sodium-ion storage in battery anodes. A promising approach to achieving this involves the oxidation of extracted coal using nitric acid prior to annealing. This pre-oxidation step introduces

functional groups and structural modifications that influence the carbon matrix, leading to increased interlayer spacing after high-temperature annealing. By treating coal with nitric acid before thermal processing, the resulting hard carbon exhibits expanded interlayer spacing, which is crucial for improved sodium-ion intercalation. This effect was confirmed through X-ray diffraction (XRD) analysis, Figures 24a and 24b, show the (002) peak shifted to lower angles, indicating a wider spacing between carbon layers. The expanded interlayer structure provides more accessible pathways for sodium-ion storage, improving the performance of hard carbon as an anode material in sodium-ion batteries. This method represents an effective strategy for tailoring the microstructure of hard carbon to meet the demands of high-capacity and efficient energy storage systems.

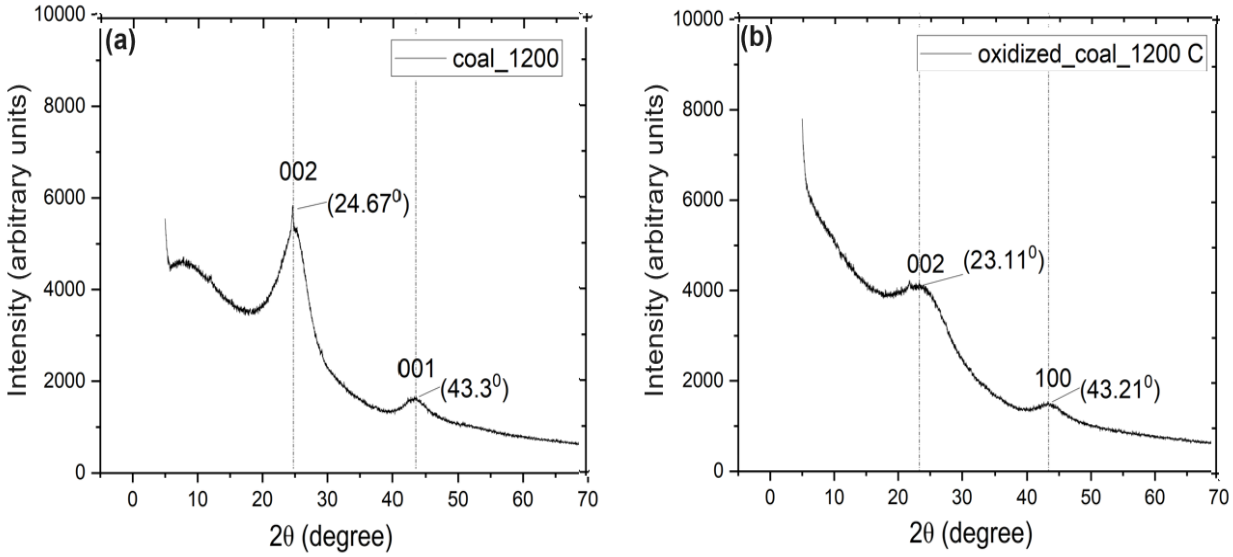

Figure 24: (a) Extracted coal char directly carbonized at 1200 °C and (b) oxidized coal char annealed at 1200 °C.

The Johnson research group has been studying ways to reduce the cost and environmental impact of GO synthesis from coal char via the nitric acid method. During these studies, HNO_3 solutions at pH 3 were precursors for new GO syntheses. After adding oxidizing agents to the pH 3 solutions, rGO was obtained. This preliminary result opened a new avenue of investigation into the possibility of making the entire GO synthesis process via the nitric acid method a green process. The results are promising, with diffractograms showing similar results to Figure 7. Raman spectroscopy results in Figure 25 attests to the synthesis of rGO.

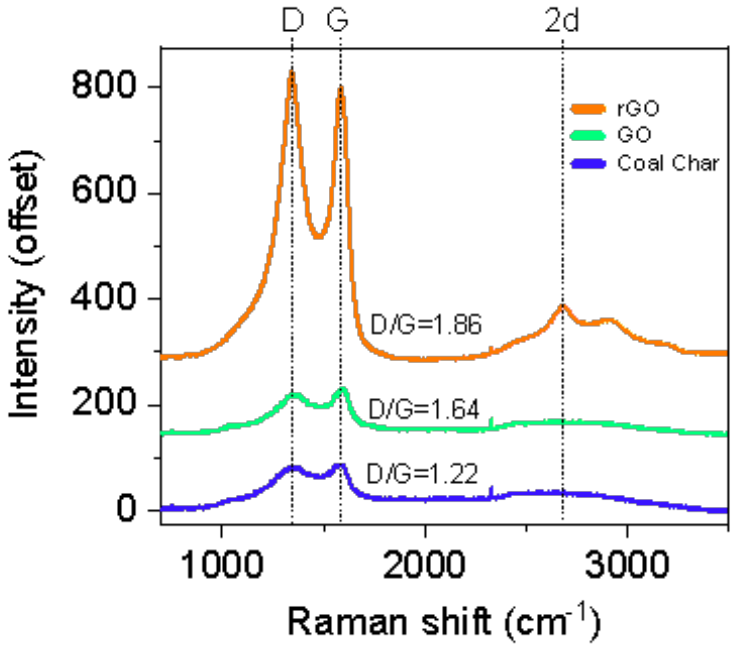

Figure 25: Raman spectra for coal char, graphene oxide (GO), and reduced graphene oxide (rGO) via recycling.

The rGO was obtained from a solution discarded in the GO synthesis with a yield of 98% w/w. One of the most effective means of reducing GO is by heating at high temperatures. The chemical method investigated is not limited by space in furnaces. To be considered green, HNO_3 solutions with pH 5, resulting from recycling nitric acid solutions with pH 3, have been neutralized with alkali metal and alkaline earth metal bases to obtain nitrates. Following this line of research, the efficiency of residual nitrates as fertilizer and the scaling of the method (large volumes) can be investigated.

Task 6.3: Battery testing results for extracted coal hard carbon annealed at 1400 °C.
Initial experiments with the extracted coal hard carbon annealed at 1400°C demonstrated promising performance in battery testing. As shown in Figure 26, at a current density of 20 mA/g, the material achieved a specific capacity close to 200 mAh/g. This is a respectable result, particularly given that the material exhibited a more graphitic nature compared to typical hard carbon known to be ideal for sodium-ion storage. While graphitic structures are less favorable for sodium-ion intercalation due to their more ordered layers and reduced interlayer spacing, the performance observed suggests that the material retains sufficient disordered regions to facilitate sodium-ion storage. This balance between graphitic characteristics and sodium-ion accessibility offers potential for further optimization, making this hard carbon a viable candidate for sodium-ion battery applications.

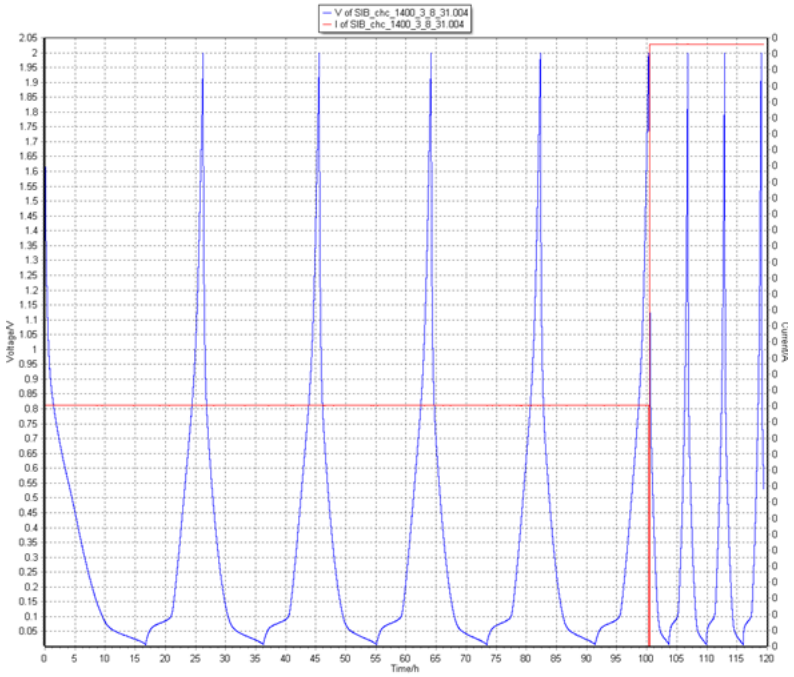

Figure 26: Battery testing.

The half cell batteries were made with three types of hard carbons (directly carbonized and peroxidized using acid and air and then carbonized) as the cathode and Na metal as the anode. The rate testing was performed at different current densities. Figure 27 shows the capacities of these three hard carbons under different current densities.

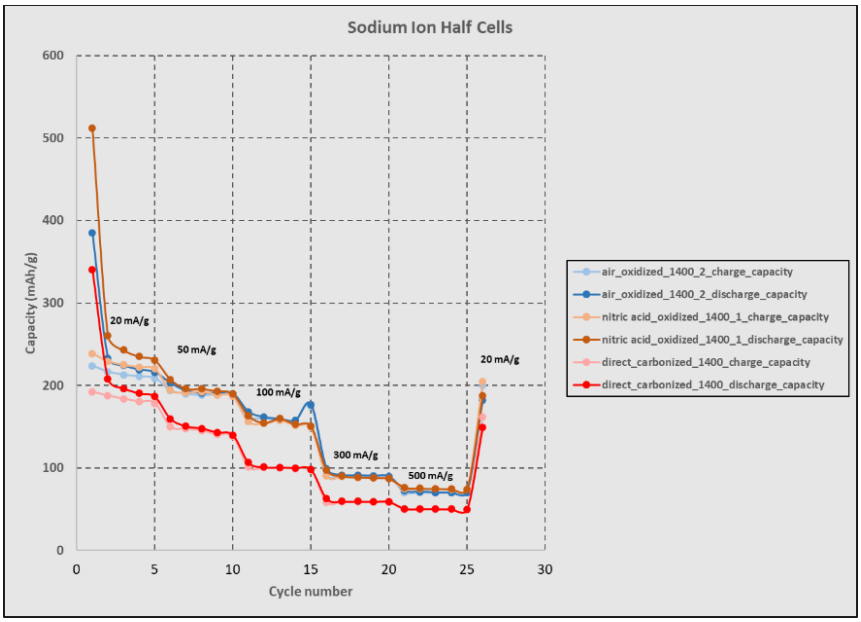

Figure 27: Rate testing.

Both acid (10 M nitric acid for 1 hour) and air oxidized (under atmospheric air at 300 ºC for three hours) hard carbons later annealed at 1400 ºC showed significantly increased capacity under all current densities compared to directly carbonized hard carbon. The Initial Coulombic Efficiency (ICE) of the directly carbonized hard carbon was 56% while the ICE of air oxidized hard carbon was 58% and that of acid oxidized hard carbon was 46%. These ICE values are too low for these hard carbons to be used in any practical full cell thus further improvement was necessary.

6.4 Oxidation procedure for pre-oxidized hard carbon

We then used a pre-oxidation strategy to present a modification process for the coal-derived hard carbon. The coal char was first extracted using 1-Methyl-2_pyrrolidone solvent to demineralize the coal char. Then approximately 3 g of coal was ground and treated with 30 mL of an acid solution, prepared by mixing 4 parts of 10 M H_2SO_4 and 1 part of 10 M HNO_3 by volume. The mixture was stirred at room temperature for 1 hour and sequentially ultrasonicated for 15 minutes. The solution was diluted with 1 L of deionized (DI) water and allowed to rest for 2 hours. The solution, as shown in Figure 28, was then centrifuged at 8000 RCF for 1 hour, replacing the supernatant with fresh DI water until a neutral pH was reached. The final product was dried at 80 °C overnight. This procedure ensures a controlled and reproducible oxidation process for further applications in material synthesis and energy storage.

Figure 28: Colloidal solution of oxidized coal after ultrasonication and resting for 2 h

The pre-oxidized and dried coal was subsequently annealed at 1400 °C under an argon flow of 200 ml/min in a tube furnace. The resulting hard carbon was labeled as 1400_LO_CHC,1400_CHC. Figure 29 below shows the diffractograms of direct carbonized extracted coal at 1400 °C (1400_CHC) and oxidized coal carbonized at 1400 °C (1400_LO_CHC).

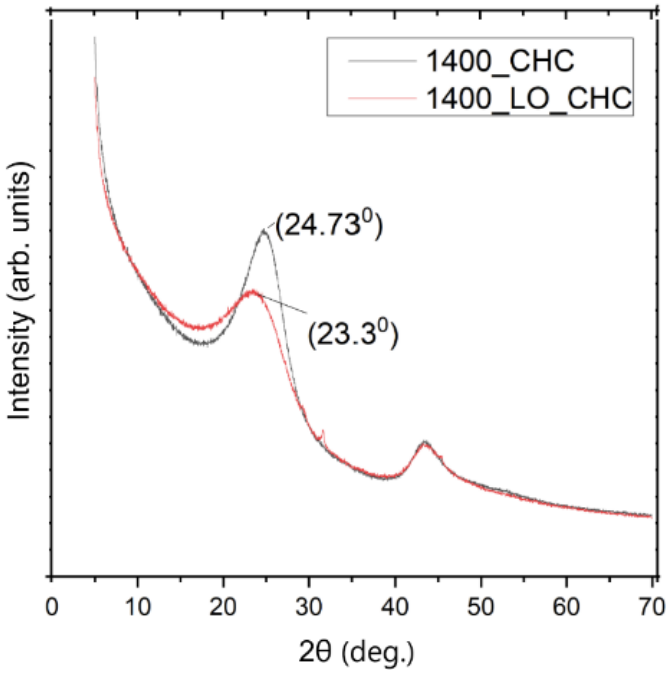

Figure 29: Diffractograms of direct carbonized extracted coal at 1400 C (1400_CHC) and oxidized coal carbonized at 1400 C (1400_LO_CHC).

The diffractograms in Figure 29 illustrate the microstructural changes induced by pre-oxidation. The 1400_CHC has an interlayer spacing of 0.36 nm, while the 1400_LO_CHC has an interlayer spacing of 0.38 nm. It is accepted in the literature that the favorable interlayer spacing for sodium

ion storage is between 0.37 nm and 0.4 nm. Thus, the 1400_LO_CHC would show better promise for higher capacity in terms of sodium storage.

6.5 Half-cell testing of Hard carbons in Sodium-ion batteries

Anodes were prepared using the fabricated hard carbons by mixing hard carbon: Super P conductive Carbon: PVDF binder in the mass ratio 8:1:1, respectively. Using a doctor blade, the slurry was mixed with NMP and coated on battery-grade copper foil. The anodes were further dried in a vacuum oven at 120 ºC. The half cells were made with sodium metal as the counter electrode. The electrolyte used was 1M NaClO4 in EC: DEC 1:1 v/v%. The coin cells were assembled inside a glovebox with H2O < 0.1 ppm and O2 < 0.1 ppm. Coin cells were then galvanostatically charged and discharged using a Maccor 4200 Battery tester. Figure 30 shows the specific capacities calculated from the results of galvanic charge-discharge tests under different current densities.

DE-FEO-0032274 – Final Technical Report

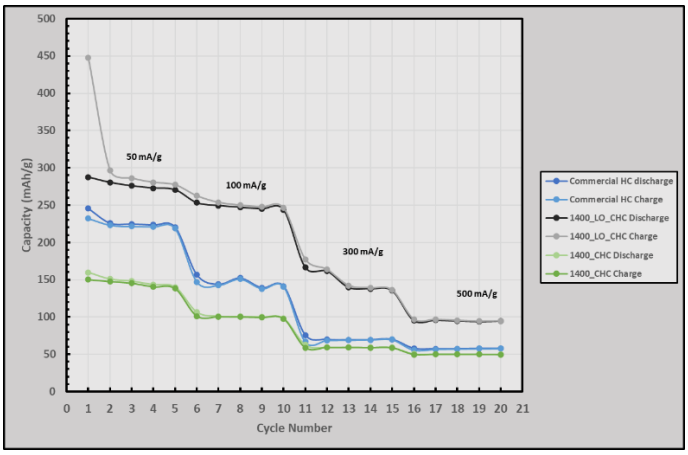

Figure 30: Rate testing of 1400_CHC, 1400_LO_CHC, and commercially purchased Hard carbon in SIB.

Even though the pre-oxidation improves the reversible capacity of the hard carbon for sodium ion storage, The initial coulombic efficiency (ICE) of this material is around 63%, which would be detrimental to the performance of a full cell. The future goal will be to employ chemical pre-sodiation on these hard carbon anodes to improve their ICE above 90% (similar processes are currently used in commercial lithium battery production). After successful pre-sodiation of the hard carbon, whole cells will be prepared using a commercially available cathode material such as sodium vanadium phosphate (NVP) to evaluate the rate capability and Coulombic efficiency under longer cycle life. Further improvements will follow in terms of optimized Solid Electrolyte Interphase (SEI) to improve the lifetime of sodium ion batteries based on hard carbon anodes.

Hard carbon microstructure of the anode material is crucial for the performance of the battery. Thus, we investigated the effect of pre-oxidation on synthesizing a more suitable microstructure for sodium ion storage. The synthesis started with 20 grams of coal char was mixed with 400 ml of N-methyl-2-pyrrolidone (NMP) and preheated at 220 ºC for two hours. After cooling, the solution was centrifuged at 8000 RCF for 30 minutes. The supernatant was vacuum filtered through a 0.45 µm pore size PTFE filter paper. The remaining NMP solvent in the sample was evaporated by placing it in a vacuum oven at 180 ºC. The extracted carbon material, designated as Ex-C, is carbonized at different temperatures, specifically 1000 ºC and 1400 ºC, for 2 hours under an argon flow of 200 ml/min.

The direct carbonized samples are abbreviated as 1000-CHC and 1400-CHC. The extracted coal char is designated as EX-C, the mildly oxidized sample, designated as OX-C, was then carbonized at 1400 ºC for 2 hours under the same conditions. The oxidized and carbonized sample 1400-LO-CHC. The schematic representation of the hard carbon formation process is displayed in Figure 31.

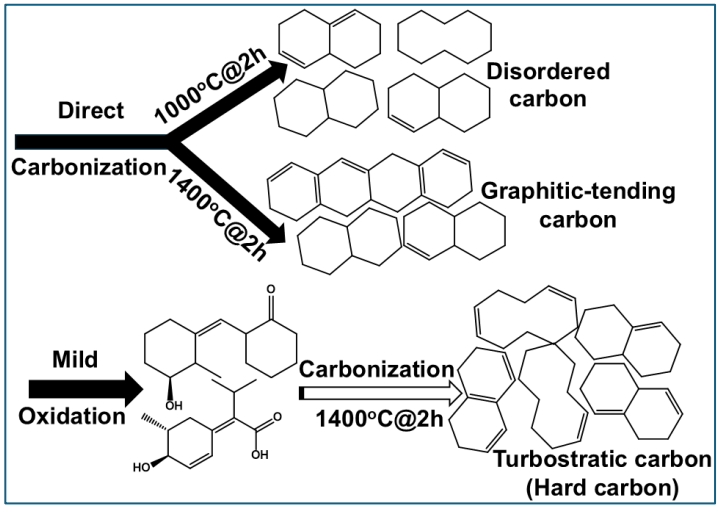

Figure 31. Schematic representation of the process of formation of hard carbon.

All the carbon materials that are synthesized as mentioned were then characterized using TGA, XRD, and Raman spectroscopy. Thermogravimetric analysis (TGA) was conducted to assess the moisture, volatile, and ash content in coal char, Ex-C, and Ox-C. As shown in Fig. 32.

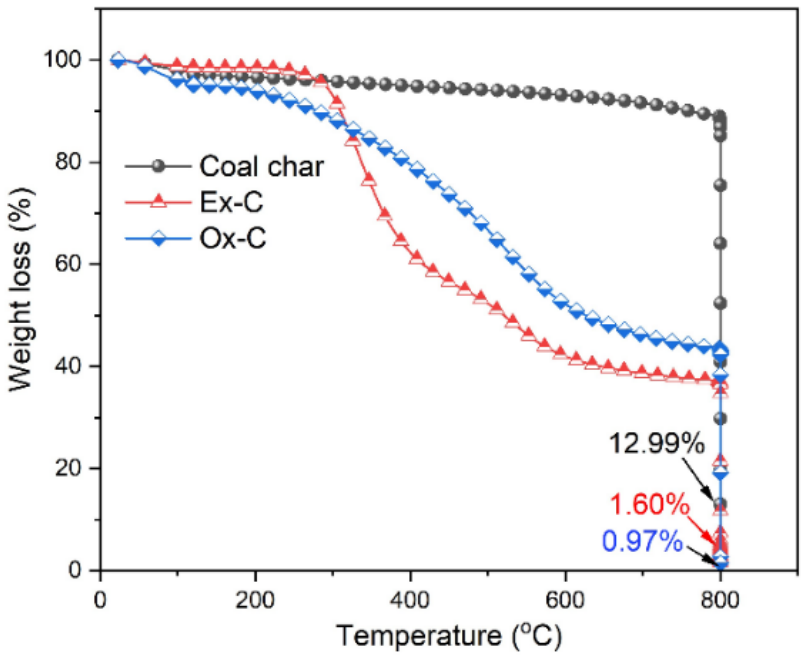

Figure 32. TGA of Coal char, Ex-C and Ox-C.

The results show that the coal char contains 12.99% ash content, indicating the presence of mineral impurities. The solvent extraction route effectively extracts a fraction of the organic matter from the coal char, reducing the ash content down to 1.6%. The morphology of carbon extracts and hard carbons are shown in Figure 33 SEM images.

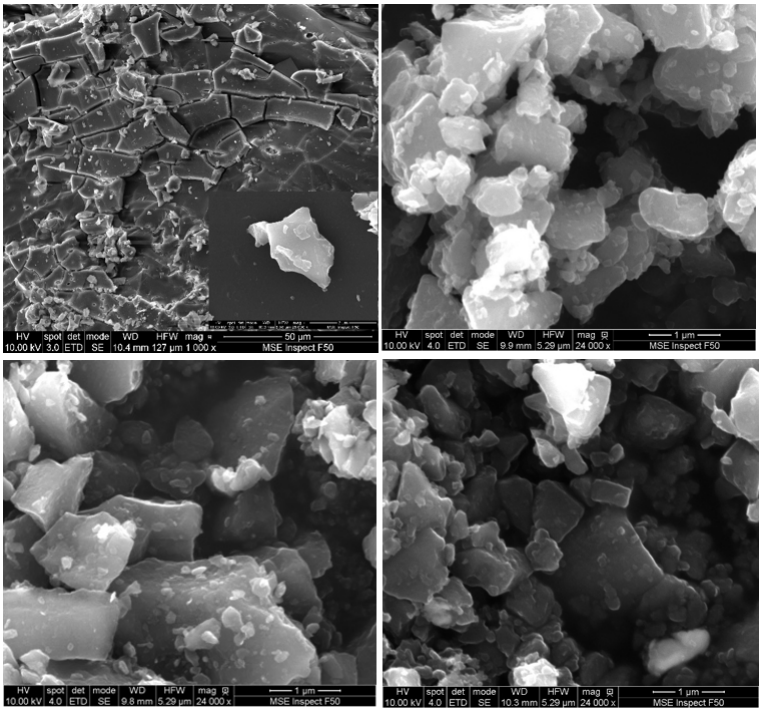

.Figure 33. SEM of (a) Ex-C, 1000-CHC, 1400-CHC, and 1400-LO-CHC.

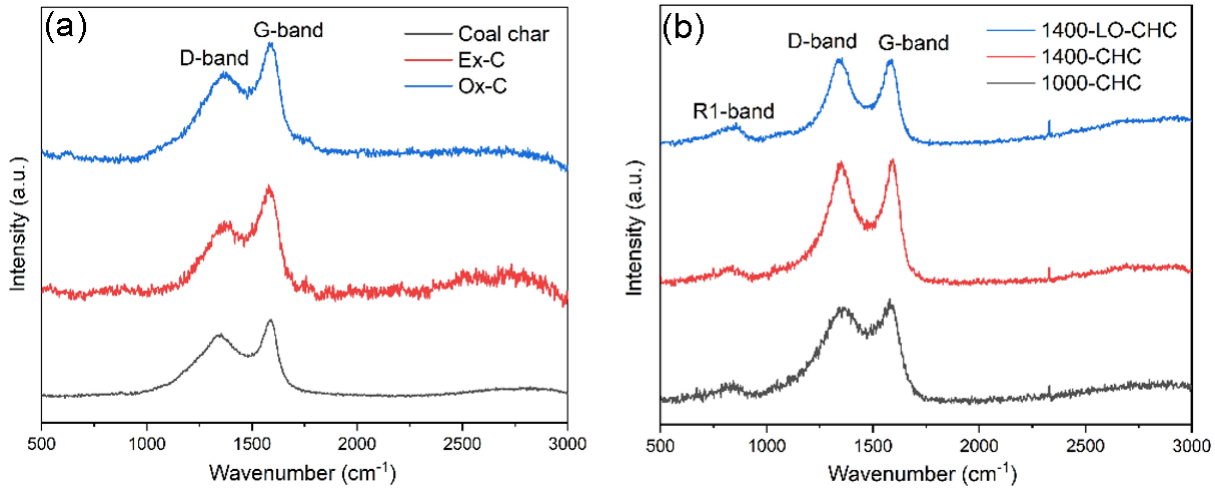

Figure 34. (a) Raman spectra of Coal char, Ex-C and Ox-C and (b) 1000-CHC, 1400-CHC and 1400-LO-CHC

Raman spectroscopy was performed on Coal char, Ex-C, Ox-C, 1000-CHC, 1400-CHC, and 1400-LO-CHC, as shown in Fig. 34. The first-order Raman spectra in carbon materials span the range of 800 cm^{-1}-2000 cm^{-1}, featuring two primary peaks: D and G, located at 1330-1350 cm and 1580 cm^{-1}-1590 cm^{-1}, respectively. The G peak is associated with E_{2g} stretching mode of the sp^2 bond, and is present for both ordered and disordered carbon, while the D peak arises from defects and disorders in the carbon lattice, breaking the 6-fold symmetry of the graphene sheet.

The level of disorder in carbon materials can be evaluated using the ratio of Raman peak intensities (I_D/I_G), which exhibits two distinct behaviors depending on the defect density. If the defect density is low, the I_D/I_G ratio decreases with decreased disorder, causing less elastic scattering. Conversely, if the defect density is high, the I_D/I_G ratio increases with increasing disorder as higher defect density leads to a more amorphous carbon structure, attenuating all Raman peaks. Equation (1) can be used to calculate the in-plane size of graphite crystallites (L_a).

$$L_a = 2.4 * 10^{-10} \lambda^4 (I_D/I_G)^{-1} \quad (1)$$

Following carbonization, the D-band peak becomes more pronounced in all samples. Fig. 35 shows a plot of (I_D/I_G) and La for all 1000-CHC, 1400-CHC and 1400-LO-CHC. The 1000-CHC sample exhibits the highest defect ratio due to pronounced structural disorder. This is attributed to more voids and open pores, which contribute to the formation of extended defects. Further increasing carbonization temperature to 1400 °C decreases the ID/IG ratio and increases the crystallite size due to closing the open pores and rearrangement of carbon atoms in graphene layers. Furthermore, the 1400-LO-CHC sample shows an increase in the crystallite size. These functional groups lead to increased hydrogen bonding between graphene layers, thus promoting the formation of pseudo-graphitic crystallites.

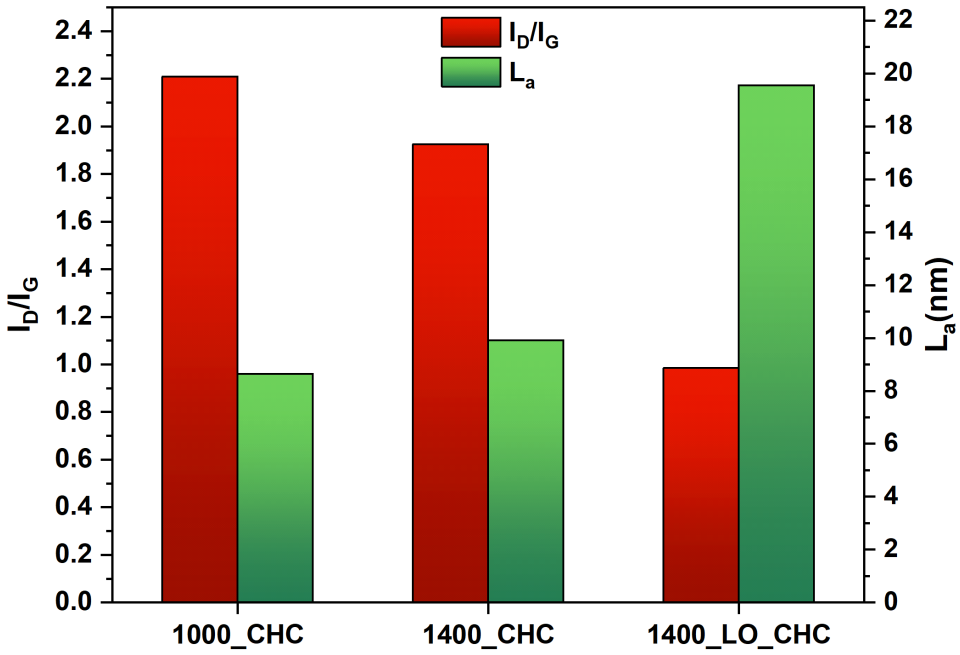

Figure 35. ID /IG ratio and La from Raman spectroscopy.

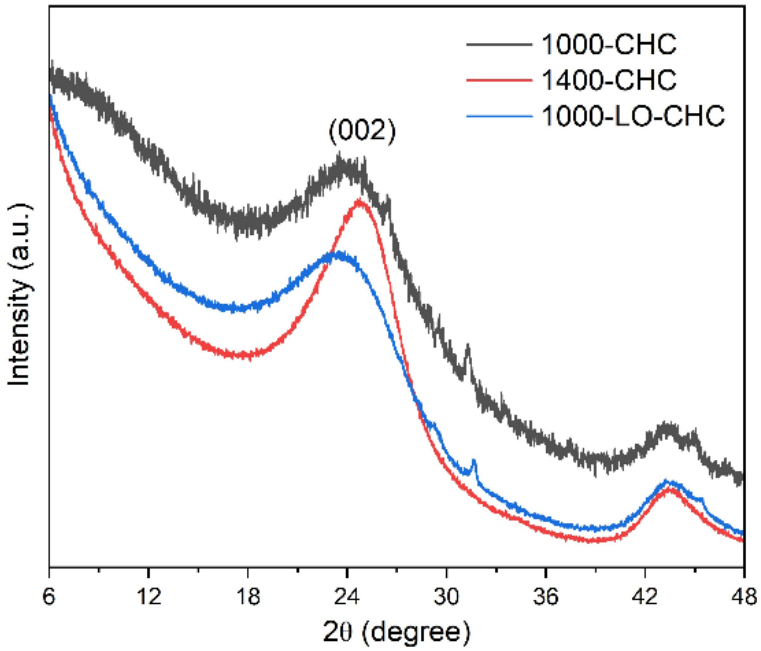

Figure 36. XRD spectra of 1000-CHC, 1400-CHC, and1400-LO-CHC.

The XRD patterns of all hard carbon samples are shown in Fig 36. As carbonization progressed with increasing temperature from 1000 ºC to 1400 ºC, the diffraction peak became sharper, indicating the formation of a short-range graphite-like structure in the direct carbonization process. However, 1400-LO-CHC maintained an amorphous character even when carbonized at 1400 ºC, suggesting that pre-oxidation prevents the formation of a short-range graphite-like structure and provides more space for Na+ storage.

In the directly carbonized hard carbon samples, the d-spacing reduces from 3.7 Å to 3.6 Å when the carbonization temperature was increased from 1000 ºC to 1400 ºC. The average longitudinal and lateral crystallite sizes also increased in 1400-CHC to 17.3 Å and 25.8 Å respectively, compared to 13.8 Å and 21.7 Å in 1000-CHC. Thus, the increased carbonization temperature reduces the average interlayer spacing of pseudographitic domains while promoting the growth of those crystallites. The 1400-LO-CHC sample displayed a broad (002) peak around 23.2° and a corresponding d spacing of 3.8 Å, suggesting that the pre-oxidation hinders the formation of the pseudo-graphitic crystallites compared to 1400-CHC and thus favors Na+ storage.

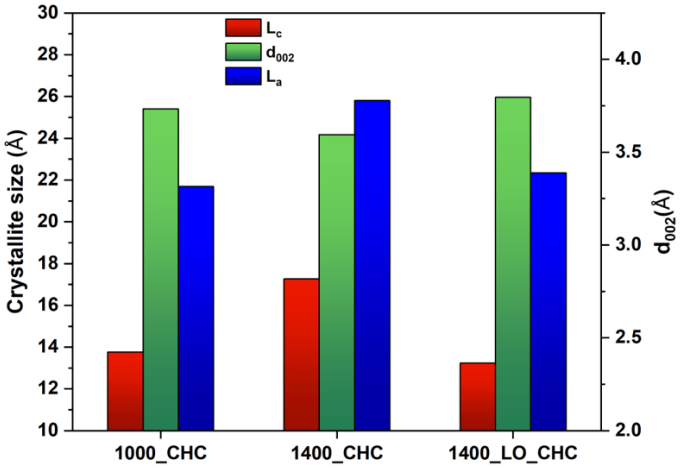

Figure 37. Longitudinal (Lc) and lateral (La) crystallite sizes and interlayer spacing (d002) of hard carbons.

The crystallite size of the 1400-LO-CHC is reduced compared to 1400-CHC, which indicates the increased turbostratic structure induced by the pre-oxidation of extracted coal (Figure 37). The galvanostatic charge-discharge (GCD) for the 1st and 5th cycles of 1000_CHC, 1400_CHC, and 1400_LO_CHC, respectively was analysed and results showed on Figures 38(a), (b), and (c).

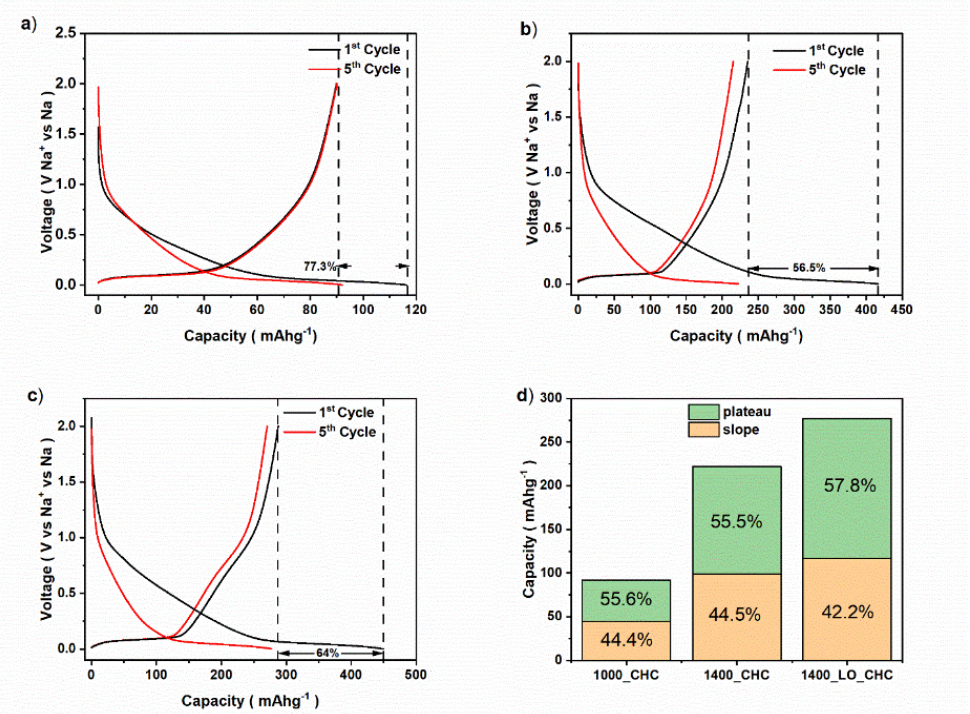

Figure 38: a) GCD charge discharge of 1000_CHC at 20 mAh/g. b) GCD charge discharge of 1400_CHC at 20 mAh/g. c) GCD charge discharge of 1400_LO_CHC at 20 mAh/g. d) Slope and Plateau Capacity of each hard carbon sample.

The 1400_CHC hard carbon exhibits a higher reversible specific capacity of approximately 222 mAh g^{-1} at a current density of 50 mA g^{-1}, compared to 92 mAh g^{-1} for 1000_CHC under the same conditions. Notably, 44.4% of the reversible capacity in both 1000_CHC and 1400_CHC originate from the slope region, as shown in Figure 38(d). The overall increased plateau capacity and slope capacity in 1400_CHC relative to 1000_CHC can be attributed to closing of pores, favoring sodium ion storage.

The peroxidized 1400_LO_CHC hard carbon demonstrates a significantly higher reversible capacity of 277 mAh g^{-1} at 50 mA g^{-1}. Despite this substantial capacity increase, the slope and plateau capacity percentages remain similar to those of 1400_CHC. This enhancement can be attributed to the more turbostratic nature of peroxidized hard carbon forming more closed pores.

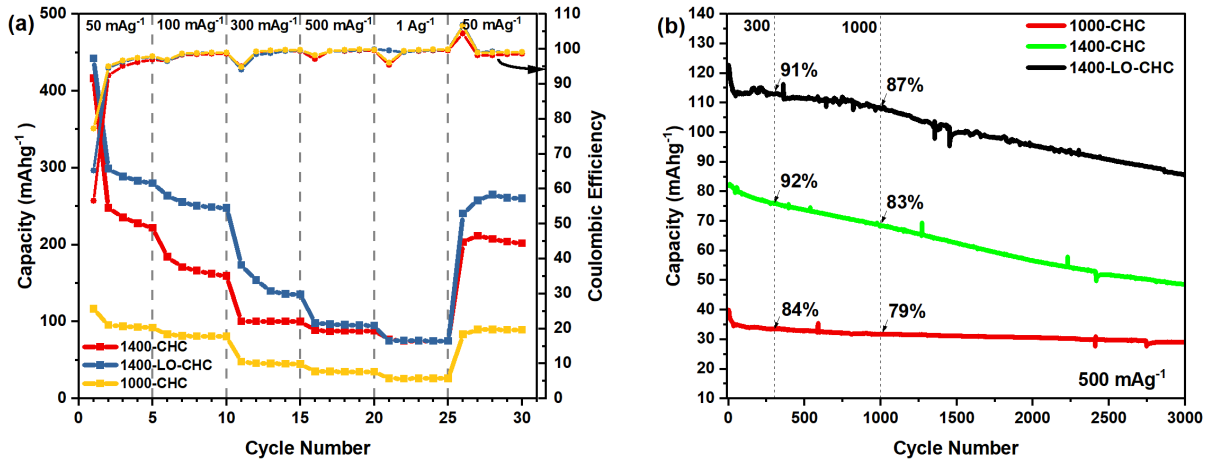

Figure 39. a) Rate testing of different hard carbon anodes. b) Long term cycling of 1400_LO_CHC at 500 mA/g.

Fig. 39(a) illustrates the rate performance of 1000_CHC, 1400_CHC, and 1400_LO_CHC at current densities of 50, 100, 300, 500 and 1000 mA g^{-1}. 1400_LO_CHC maintains a significantly higher reversible capacity across all current densities, except at 500 mA g^{-1} and 1 A g^{-1}, where both 1400_CHC and 1400_LO_CHC exhibit similar specific capacities of approximately 100 mAh g^{-1}. 1000_CHC on the other hand showed a significantly lower specific capacity under all current densities.

Long-term cycling performance was evaluated for the 1000_CHC, 1400_CHC, and 1400_LO_CHC ,1400_LO_CHC anode in a half-cell configuration at a current density of 500 mA g^{-1}.1000_CHC and 1400_LO_CHC loses close to 10% of its initial capacity during the first 40 cycles and stays relatively stable on successive cycles. This behavior is due to solid electrolyte interphase (SEI) formation, electrolyte decomposition, and degradation of active material. Overall, 1400_LO_CHC retained approximately 87% of its reversible capacity after 1000 cycles at 500 mA g^{-1}, demonstrating excellent long-term stability.

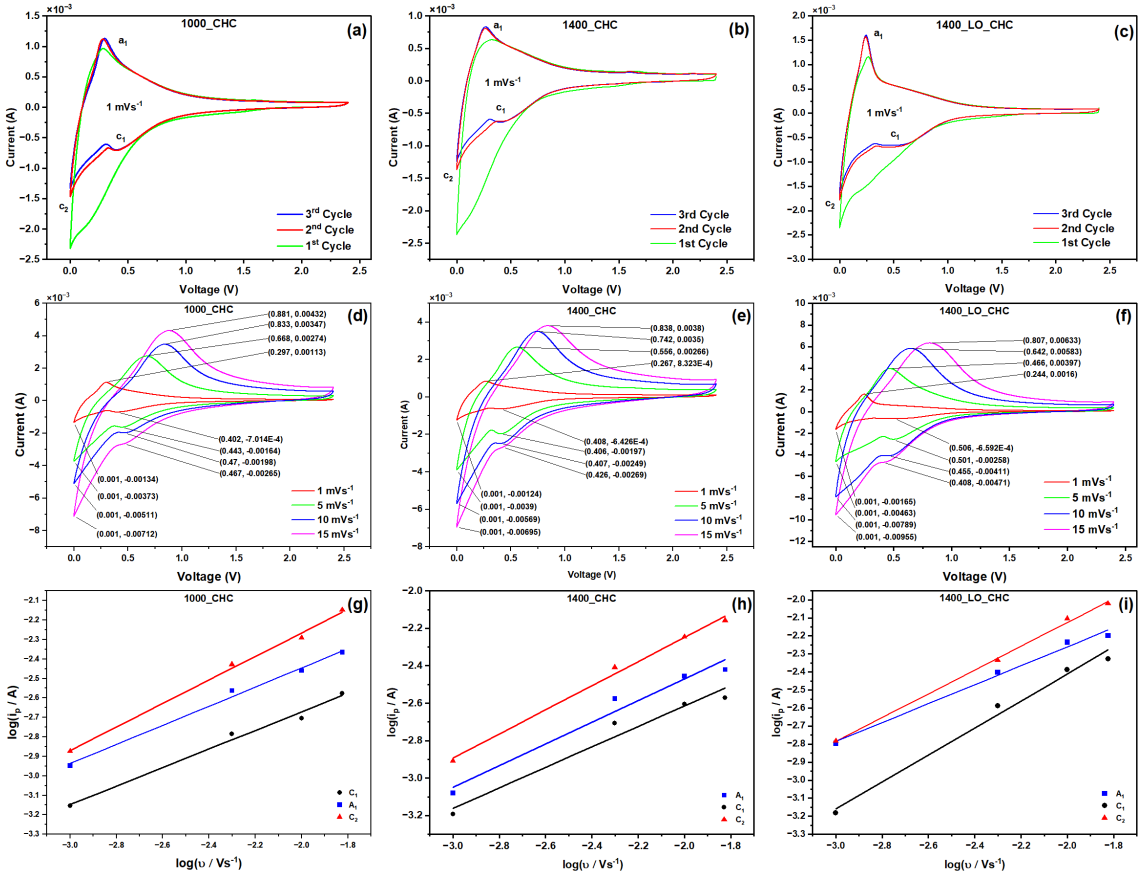

Figure 40. a-c) CV of 1000_CHC, 1400_CHC and 1400_LO_CHC at 1 mV/s. d-f) CV of 1000_CHC, 1400_CHC and 1400_LO_CHC at different scan rates. g-i) log-log plot of scan rate vs peak current for c_1, c_2 and a_1 peaks.

Fig. 40 (a), (b), and (c) show the results of cyclic voltammetry (CV) performed at 1 mV/s for 1000_chc, 1400_chc, and 1400_LO_CHC, respectively. During the 1st cathodic scan of all three half cells, there is a broad irreversible peak appearing between 0.5 V and 0.1 V, which disappears from subsequent scans. This irreversible broad peak is attributed to SEI formation and electrolyte decomposition. In all three hard carbons, two cathodic peaks are visible: one broad peak between 0.7 V and 0.2 V, which is named c_1, and another sharp peak around 0.001 V, which is named c_2.

The reversible cathodic peak c_1 can be attributed to the adsorption of sodium ions, and the c_2 peak is attributed to the pore filling of sodium ions. In all three hard carbons an anodic peak appears between 0.2 V and 0.5 V which is designated as a_1. The a_1 anodic peak is attributed to the deintercalation of sodium ions from the hard carbon.

$$i_p = a\nu^b \quad (2)$$

Fig. 40 (d), (e), (f) show the results of CV scans done at 1 mV/s, 5 mV/s, 10 mV/s, and 15 mV/s for 1000_CHC, 1400_CHC, and 1400_LO_CHC half cells, respectively. With increasing scanning

rates, the current also increases. The log value of peak currents ($\log(i_p)$) of c_1, c_2 and a_1 are plotted against log value of scan rates ($\log(\nu)$) in Fig. 40 (g), (h), (i).

The peak current can be related to the scan rate using Equation 2. The slopes of fitted lines correspond to the constant b. If the constant b is equal to 0.5, the reaction is diffusion controlled, and if b is equal to 1, it is adsorption controlled. The results summarized in Table 7 show that all hard carbons show diffusion-controlled reactions when intercalating and deintercalation sodium ions.

Table 7. Fitted parameters for the impedance spectroscopy measurements using the equivalent circuit in Figure 41.

	RMSE	R_s	R_{SEI}	C_{SEI}	C_{dl}	R_{ct}	W
1000_chc	0.4069	4.0108	13.7234	0.0025	4.01E-06	3.09542	193.3903
1400_chc	0.5135	9.1787	29.9210	0.002247	1.41E-05	4.1245	132.1866
1400_lo_chc	0.1835	6.6387	39.5161	0.001821	2.59E-05	9.1394	64.2429

The electrochemical impedance spectroscopy (EIS) was carried out to investigate the electrochemical properties of the hard carbons. The Nyquist plots of the three different hard carbon working electrodes are shown in Fig. 41. The equivalent circuit used to fit the impedance spectra is shown in the inset. The fitting parameters are summarized in Table 8. Resistance of the SEI layer (R_{SEI}) significantly changes among the different hard carbons.

The increased RSEI value of the 1400_lo_chc is attributed to the larger SEI formed due to the increased pore size and the increased double layer capacitance (Cdl) is an indication of the increased surface area of the 1400_lo_chc hard carbon. The charge transfer resistance (Rct) is increased in the 1400_lo_chc compared to 1000_chc because the former has more surface adsorption behavior. 1400_lo_chc also shows significantly less Warburg impedance (W) due to the increased diffusion of sodium ions in the hard carbon.

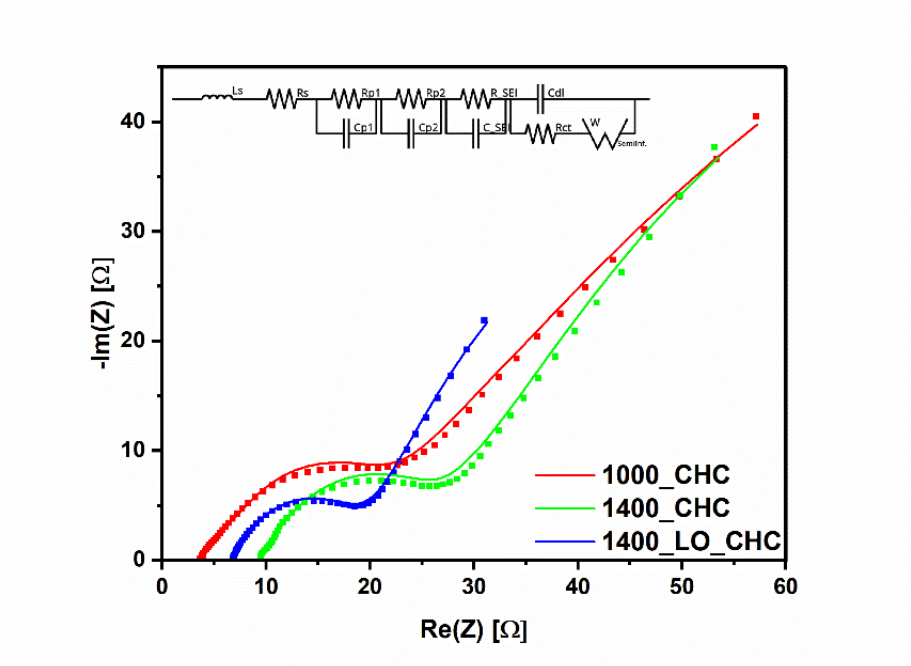

Figure 41. Measured EIS results (symbol). Fitted equivalent circuit simulation (solid line).

The electrochemical performance of hard carbons derived from coal char prepared from the solvent-extracted method has been investigated. The structural and surface morphologies of hard carbons are significantly influenced by carbonization temperature and pre-acid treatment of extracted carbon.

The hard carbon sample carbonized at 1400 °C after mild pre-oxidation (1400-LO-CHC) demonstrated a specific capacity of 277 mAh g^{-1} at 50 mA g^{-1}, compared to the hard carbon sample directly carbonized at 1400 °C (1400-CHC), which showed a specific capacity of 222 mAh g^{-1} at 50 mA g^{-1}. This capacity enhancement through pre-oxidation is attributed to oxygen functional groups inhibiting the stacking of aromatic layers, thereby enhancing the turbostratic nature of the hard carbon. Notably, the 1400-LO-CHC sample maintained ~ 87% of its reversible capacity after 1000 cycles at a current density of 500 mA g^{-1}, demonstrating exceptional long-term stability at high current densities.

Future work will be done to address any shortcomings of the synthesis process and the electrochemical performance of the resulting hard carbon. The acid pre-oxidation route of this method diminishes the yield of the oxidized extracted coal by close to 30% of the extracted coal mass used. Another shortcoming of this hard carbon is the lower ICE, which is close to 65%. As a solution, we are investigating the use of pre-sodiation before assembling the half cells (a common method in commercial lithium ion battery production to overcome this with graphite and other anode materials). Table 5 show the capacity and current density cycle stability for different samples quoted in the literature and from this work.

Table 8. Capacity, current density cycle stability and references.

Sample	Capacity ($mAhg^{-1}$)	Current Density (Ag^{-1})	Cycle stability	Ref.
Soft carbon coal derived hard carbon	320	0.01	80% after 400 cycles at $1Ag^{-1}$	[18]
Bituminous coal de rivedcarbon	287.1	20 mAg^{-1}	96.1% after 200 cycles at 50 mAg^{-1}	[19]
Porous flaky HC de rived from coal	303.6	30 mAg^{-1}	54.5% over 1000 cycles at 100 mAg^{-1}	[20]
Coal based hard carbon	201	2 Ag^{-1}	96.2% over 500 cycles at 1Ag−1	[21]
Coal based hard carbon with fast carbonization	292	0.1C	74% at 2.0C after 1000 cycles	[22]
$Zn_2(OH)_2CO_3$ assisted coal derived hard carbon	325.3	0.03 Ag^{-1}	83.5% over 500 cycles at 0.1 Ag^{-1}	[23]
Coal derived Hard Carbon	250	20 mAg^{-1}	>80% at 200 cycle at 100 mAg^{-1}	[24]
Hard carbon derived from long-flame coal	254	20 mAg^{-1}	72% after 1000 cycles at 500 mAg^{-1}	[25]
Coal derived Hard Carbon	304.7	30 mAg^{-1}	96.0% after 300 cycles at 100 mAg^{-1}	[26]
Hard Carbon from coal char	277 $mAhg^{-1}$	50 mAg^{-1}	87% over 1000 cycles at 500 mAg^{-1}	This work

X-ray photoelectron spectroscopy (XPS) was utilized to evaluate the surface composition of coal char following the pre-oxidation process. Figure 42 presents the XPS survey spectra for the mildly

oxidized sample (OX-C), the extracted carbon material (EX-C), and coal char (a), as well as high-resolution C1s peaks fitted to coal char (b), EX-C (c), and OX-C (d).

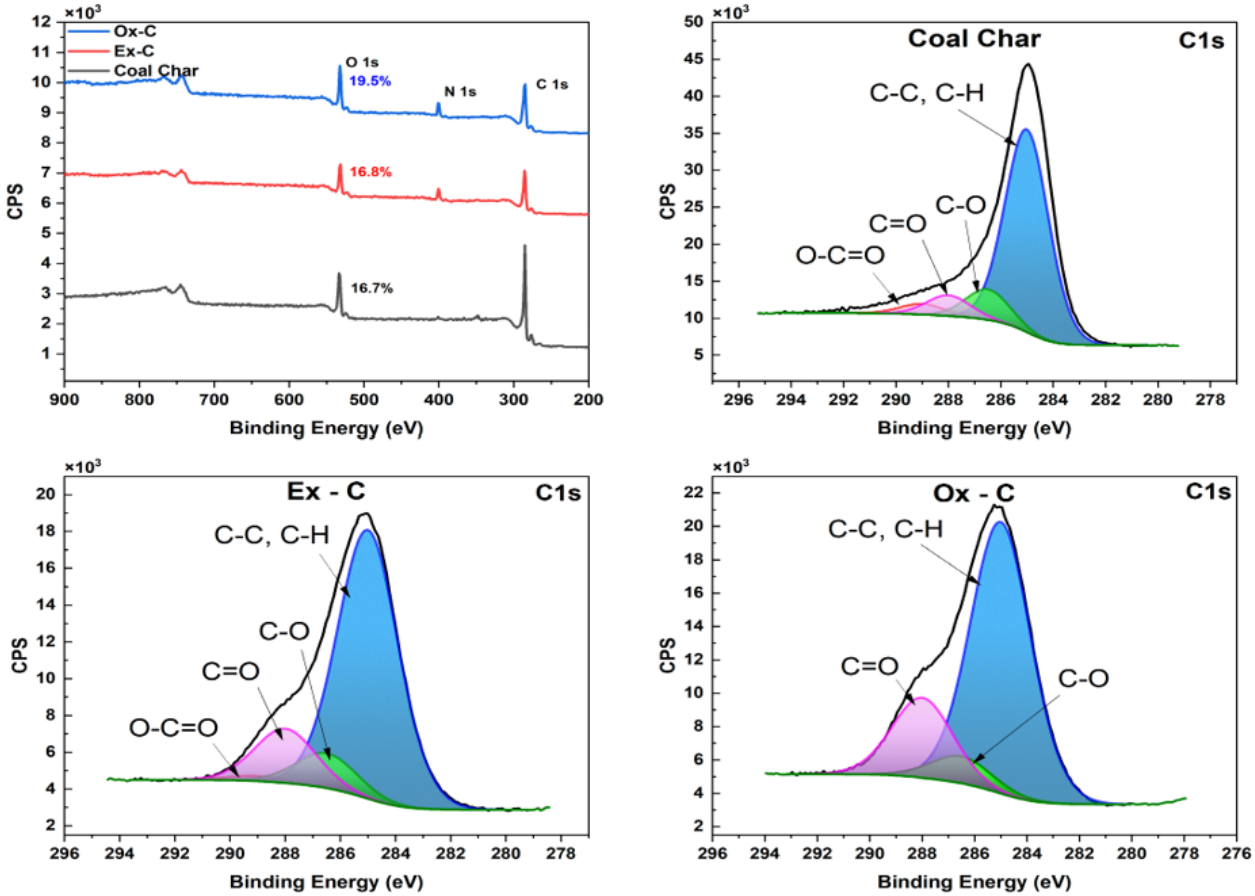

Figure 42. (a) XPS survey spectrum of coal char, Ex-C and Ox-C. (b) High-resolution C1 s, (c) High-resolution C1S XPS spectra of Ex-C. (d) High-resolution C1S XPS spectra of Ox-C.

The elemental composition (At.%) for coal char, Ex-C and Ox-C are shown in Tables 9 (survey spectra). In Table 10 are shown the chemical bond composition (high-resolution fitted C1 peaks). The data show that the pre-oxidation procedure was capable of introducing increased concentration of (C=O) bonds to the Ox-C sample.

Table 9. XPS elemental composition analysis

Sample Identifier	Name	Position	FWHM	Area	% At. Conc.
Coal-char	C 1s	284.94	2.02	98454.94	83.3
	O 1s	532.54	3.53	57816.77	16.7
Ex-C	C 1s	285.03	2.99	53895.84	73.73
	O 1s	531.73	2.8	36075.15	16.84
	N 1s	400.23	2.4	12411.61	9.43
Ox-C	C 1s	285.25	3.26	64938.45	71.28
	O 1s	531.65	2.85	51960.45	19.47
	N 1s	400.25	2.27	15172.52	9.25

Table 10. XPS bond composition analysis

Sample Identifier	Name	Position	FWHM	Area	% At. Conc.
Coal-char	C-C, C-H	285	1.95	59895.88	60.91
	C-O	286.5	1.95	8984.61	9.14
	C=O	288	1.95	6098.25	6.2
	O-C=O	289	1.95	3154.72	3.21
Ex-C	C-C, C-H	285	2.59	39926.39	74.09
	C-O	286.5	2.59	5157.05	9.57
	C=O	288	2.59	8067.48	14.97
	O-C=O	289	2.59	737.6	1.37
Ox-C	C-C, C-H	285	2.71	46684.6	71.74
	C-O	286.5	2.71	4638.73	7.13
	C=O	288	2.71	13748.13	21.13

Pre-oxidation effects are confirmed by the measured oxygen atomic concentrations 16.7% in coal char, 16.8% in Ex-C, and a noticeable increase to 19.5% in Ox-C, indicating successful incorporation of oxygen-containing functional groups. High-resolution C-1s spectra (Fig.42) further revealed dominant C=O bond formation in Ox-C, consistent with FTIR results showing enhanced carbonyl and hydroxyl vibrations. Detailed atomic concentrations are provided in Table 9. The increased functional groups in the Ox-C results in a more turbostratic microstructure when carbonized, resulting in a high specific capacity hard carbon

Tasks and Milestones

Milestone Title/Description	Planned Completion Date	Actual Completion Date	Comments
2. Flash Pyrolyses of coal to coal char	Feb 2024	Feb 2024	This step has been carried out successfully.
3. GO quality – Raman D/G-ratio higher than coal char, and >1	Jun 2024	Jully (2025) Completed	This step has been carried out successfully.
4. Synthesis of rGO	Nov 2024	September (2025) Completed	This step has been carried out successfully.
5.Testing as concrete additive/cement replacement	Mar 2025	August (2025) Completed	This step has been carried out successfully.
6. Sodium-ion battery fabrication /test	Jun 2025	August (2025) Completed	This step has been carried out successfully.

Project DOE summary

1. Overview

This project demonstrated the conversion of Powder River Basin coal into valuable graphene-based materials, including graphene oxide, reduced graphene oxide, and hard carbon anodes for sodium-ion batteries. Major outcomes include: a reproducible flash pyrolysis process for high-carbon coal char; scalable synthesis of graphene oxide with high yields; production of quality reduced graphene oxide; incorporation of graphene oxide into concrete for up to 19% stronger compressive strength; and development of hard carbon anodes achieving 277 mAh/g and stable performance over 1000 cycles. These results confirm the feasibility of using coal-derived carbon for construction and energy storage, aligning with DOE goals for high-value coal products.

2. Accomplishments and Technical Outcomes

2.1. Flash Pyrolysis of Coal to Coal Char

A two-step pyrolysis process (500°C pre-pyrolysis followed by 900–1000°C flash pyrolysis) was optimized. Resulting coal char met success criteria (Fixed carbon: 76–80%, Devolatilization: 80–81%, Ash content: ~11.4%)

2.2. Graphene Oxide (GO) Synthesis and Optimization

Graphene oxide was produced via a modified nitric acid method with sonication with Raman D/G ratio >1 achieved, confirming structural disorder consistent with graphene oxide. The process improvements increased yield from 120 g/week to 1000 g/week. The Economic analysis estimated GO production cost at ~$3.78/g at lab scale, with reduction in cost at industrial scale. Recycling of nitric acid waste streams was demonstrated, moving toward a more economical synthesis route.

2.3. Reduced Graphene Oxide (rGO) Production

Reduced graphene oxide was produced via thermal reduction (1000°C under inert atmosphere) showing a sharp (002) XRD peak at 26.5° confirmed graphitic stacking. Raman spectroscopy showed increased D/G ratio post-reduction, indicating defect introduction and oxygen removal.

2.4. GO as Concrete Additive

GO was incorporated into concrete as both a cement replacement and an additive with optimal loading: 0.25% GO by weight of cement. The addition of GO caused strength improvements (Compressive strength increasing up to 19% (additive case, w/c = 0.5); Flexural strength increasing up to 27% ; Split tensile strength increasing up to 20% and workability decreased with GO addition but remained within acceptable ranges for placement.

2.5. Hard Carbon Anodes for Sodium-Ion Batteries

The production of high-performance hard carbon anodes involved a two-step process: first, solvent extraction of coal char to remove mineral impurities, followed by a strategic pre-oxidation using nitric acid. This pre-oxidation step was pivotal in tailoring the carbon microstructure, successfully increasing the interlayer spacing to ~0.38 nm to facilitate sodium-ion storage. The best-performing anode, a partially oxidized and annealed hard carbon, exceeded the performance criteria set in the proposal - reversible capacity at a current density of 20 mA g-1 reached ~ 300 mAh g-1, the ion extraction voltage was ~0.1 V vs Na/Na+, and the coulombic efficiency remained ~99% after 15 cycles on the cycling stability test at 20 mA g-1.

Further results exceeded these goals as the anode achieved a notable specific capacity of 277 mAh/g at 50 mA/g and exhibited robust long-term stability, retaining approximately 87% of its capacity after 1,000 cycles at 500 mA/g. While these results are promising, further development is needed to address the initial coulombic efficiency (ICE) of ~65%; implementing a pre-sodiation protocol is the planned route to overcome this limitation.

3. Products and Outputs

Project outputs include significant knowledge dissemination, with two journal submissions and multiple conference presentations. Substantial material deliverables, including ~5 kg of GO and ~1 kg of rGO, were transferred for application studies. The work yielded optimized synthesis protocols and a preliminary scale-up analysis, demonstrating a credible path toward industrial translation. Success was enabled by effective collaboration between Iowa State University (Materials Science and Engineering) and the University of Wyoming (Civil Engineering).

3.1. Publications, conference papers, and presentations

Isuru Gusthigngnawadu and Patrick A. Johnson, Improving the Initial Coulombic Efficiency Through Direct Contact Pre-Sodiation, A05-0851, ECS Chicago, 2025.

Vineeta Shukla, José Mario Ferreira Jr., Iftekhar Alam Dipta, Kam Ng, Patrick Alfred Johnson, Optimization of cement ratio with coal-derived GO and rGO, (in preparation).

Isuru Gusthigngnawadu , Vineeta Shukla , Patrick A. Johnson, A Hard Carbon Anode with Long-Term Cycling Stability from Pre-Oxidized Solvent Extracted Coal, (submitted).

José Mario Ferreira Jr, Vineeta Shukla, Bryce L. Wilson and Patrick Alfred Johnson, Recent Developments in Electrochemical Exfoliation for Graphene Oxide Production, (in preparation).

José Mario Ferreira Jr, Vineeta Shukla, Bryce L. Wilson and Patrick Alfred Johnson, Electrochemical-Assisted Synthesis of Reduced Graphene Oxide: A Fast, and Cost-Effective Alternative, Under process.

4. Impact Statement

This project has demonstrated a viable pathway to transform low-value coal into high-performance materials for infrastructure and clean energy storage. The successful use of graphene oxide in concrete could lead to stronger, more durable infrastructure with reduced cement consumption. Coal-derived hard carbon anodes offer low-cost, sustainable material for next-generation sodium-ion batteries, supporting grid storage and electric vehicle markets. The project also contributes to U.S. energy security by creating new markets for domestic coal.

5. Challenges and Future Work

The project successfully validated the technical feasibility of converting coal into high-value carbon materials. Major challenges ahead are lowering GO production costs with scalable methods and acid recycling, boosting hard carbon anode efficiency for batteries, and refining concrete mixes to include GO while maintaining workability. Future work should focus on pilot-scale demonstrations, targeted electrochemical optimization, comprehensive sustainability and

economic analyses, and the exploration of new product streams to fully realize the commercial potential of coal-derived graphitic materials.

6. Budget Summary

Category	FY2024 DOE Funds	FY2025 DOE Funds	Total DOE Funds
ISU Direct	$309,745.24	$277,794.75	$587,539.99
Subaward to UW	$75,984.64	$336,289.67	$412,274.31
Total DOE	$385,729.88	$469,687.11	$999,814.30
Cost Share	$103,694.36	$146,305.46	$249,999.82

7. Workforce Development

This project served as an essential training ground for emerging specialists in sustainable materials and energy, making a significant contribution to workforce development. A committed team, consisting of research scientists (José Ferreira, ISU; Elijah Ellis, UW), a postdoctoral scholar (Vineeta Shukla), and Ph.D. students (Isuru Gusthignngnawadu, ISU; Iftekhar Dipta, UW). Several undergraduate researchers were also funded on this project. Students received interdisciplinary training in the full technology value chain, from coal pyrolysis and graphene synthesis to characterization and applied testing. Collaboration with the University of Wyoming further improved crucial interdisciplinary communication abilities. Through direct involvement in projects that repurpose fossil resources into materials for sustainable infrastructure and energy storage, the team developed a robust problem-solving approach, strengthening their capacity to address global energy and sustainability challenges. DOE financial support empowered students and researchers to develop new materials, adding value to low-cost precursor materials in the production of high-value-added cementitious materials and batteries. The success of this project is evidenced not only by its technical achievements but also by the cultivation of a skilled, collaborative, and confident group of professionals prepared to lead future innovations, thereby maximizing the long-term impact of DOE’s investment.

8. Conclusion

The funding for this project enabled the synthesis and characterization of graphene oxide and reduced graphene oxide at an estimated cost 10 times lower than the market cost. To this end, a dedicated laboratory was created for the synthesis and characterization of these materials, as well

as for the development of alternative, environmentally friendly processes of graphene oxide and reduced graphene oxide. The project successfully met all stated technical milestones, proving that coal-derived graphene materials can enhance concrete performance and serve as viable anode materials for sodium-ion batteries. The work provides a foundation for further development and commercialization of coal-based carbon products, aligning with DOE's goals for fossil energy innovation and sustainable materials development.

REFERENCES

[1] ASTM C150/C150M-22: ASTM Standard Specification for Portland Cement. ASTM International, West Conshohocken, PA, (2022).

[2] ASTM C33/C33M-24: ASTM Standard Specification for Concrete Aggregates. ASTM International, West Conshohocken, PA, (2024).

[3] ASTM C127-15: ASTM Standard Test Method for Relative Density (Specific Gravity) and Absorption of Coarse Aggregate. ASTM International, West Conshohocken, PA, (2015).

[4] ASTM C29/C29M-23: ASTM Standard Test Method for Bulk Density ("Unit Weight") and Voids in Aggregate. ASTM International, West Conshohocken, PA, (2023).

[5] ASTM C566-19: ASTM Standard Test Method for Total Evaporable Moisture Content of Aggregate by Drying. ASTM International, West Conshohocken, PA, (2019).

[6] ASTM C136/C136M-19: ASTM Standard Test Method for Sieve Analysis of Fine and Coarse Aggregates. ASTM International, West Conshohocken, PA, (2019).

[7] ASTM C39/C39M-23: ASTM Standard Test Method for Compressive Strength of Cylindrical Concrete Specimens. ASTM International, West Conshohocken, PA, (2023).

[8] ASTM C496/C496M-17: ASTM Standard Test Method for Splitting Tensile Strength of Cylindrical Concrete Specimens. ASTM International, West Conshohocken, PA, (2017).

[9] ASTM C78/C78M-22: ASTM Standard Test Method for Flexural Strength of Concrete (Using Simple Beam with Third-Point Loading). ASTM International, West Conshohocken, PA, (2022).

[10] ASTM C192/C192M-19: ASTM Standard Practice for Making and Curing Concrete Test Specimens in the Laboratory. ASTM International, West Conshohocken, PA, (2019).

[11] ASTM C143/C143M-20: ASTM Standard Test Method for Slump of Hydraulic-Cement Concrete. ASTM International, West Conshohocken, PA, (2020).

[12] L. Djenaoucine, A. Picazo, M.A. de la Rubia, J.C. Gálvez, A. Moragues, Effect of graphene oxide on the hydration process and macro-mechanical properties of cement, Boletín de La Sociedad Española de Cerámica y Vidrio 63 (2024) 294–303. https://doi.org/10.1016/j.bsecv.2024.03.001.

[13] X. Li, C. Li, Y. Liu, S.J. Chen, C.M. Wang, J.G. Sanjayan, W.H. Duan, Improvement of mechanical properties by incorporating graphene oxide into cement mortar, Mechanics of Advanced Materials and Structures 25 (2018) 1313–1322. https://doi.org/10.1080/15376494.2016.1218226.

[14] B. Lian, S.D. Luca, Y. You, S. Alwarappan, M. Yoshimura, V. Sahajwalla, S. C. Smith, G. Leslie, R. K. Joshi, Extraordinary water adsorption characteristics of graphene oxide, Chemical Science 9 (2018) 5106–5111. https://doi.org/10.1039/C8SC00545A.

[15] Yolanda De Abreu, Prashanth Patil, Andres I. Marquez, Gerardine G. Botte, Characterization of electrooxidized Pittsburgh No. 8 Coal, Volume 86, Issue 4, March 2007, Pages 573-584.

[16] Yali Liu, Xiurong Zhao, Jianli Li, Dan Ma, Runping Han, Characterization of biochar from pyrolysis of wheat straw and its evaluation on methylene blue adsorption, Desalination and Water Treatment Volume 46, Issues 1–3, August 2012, Pages 115-123.

[17] Jun Xu, Qichen He, Zhe Xiong, Yun Yu, Shu Zhang, Xun Hu, Long Jiang, Sheng Su, Song Hu, Yi Wang, Jun Xiang, Energy Fuels 2021, 35, 2870−2913.

[18] X. Jin, H. Ma, G. Liu, X. Zhang, D. Wang, D. Mo, J. Xie, L. Feng, M. Wu, B. Su, et al., Pore structure modulation and defect engineering of soft carbon@ coal-derived hard carbon for enhanced sodium storage application in sibs, Inorganic Chemistry Frontiers (2025).

[19] G. Liu, J. Yuan, H. Li, Z. Li, C. Hu, X. Qiao, M. Wang, B. Yuan, P. Zhang, Z. Wu, Multieffect preoxidation strategy to convert bituminous coal into hard carbon for enhancing sodium storage performance, ACS Applied Materials & Interfaces 16 (35) (2024) 46226–46236.

[20] X.-Y. Wang, K.-Y. Zhang, M.-Y. Su, H.-H. Liu, Z.-Y. Gu, D. Dai, B. Li, J.-W. Wang, X.-Y. He, X.-L. Wu, Coal-derived flaky hard carbon with fast Na+ transport kinetic as advanced anode material for sodium-ion batteries, Carbon 229 (2024) 119526.

[21] S. Hou, D. Zhang, Y. Lei, Y. Zhou, D. Yang, P. Dong, B. Xu, B. Yang, F. Liang, Regulating closed pore structure of coal-based hard carbon anode by preoxidation for high-rate performance sodium-ion batteries, Langmuir (2025).

[22] H. Wang, F. Sun, Y. Wang, D. Wu, J. Gao, J. Wang, J. Gao, Thermal shock reducing amorphous carbon ratio in hard carbon for improved rate capability of sodium ion storage, Carbon 229 (2024) 119528.

[23] W.-Y. Qian, X.-Y. Zhou, X.-Y. Liu, M.-Y. Su, K.-Y. Zhang, X.-L. Wu, Breakage of the dense structure of coal precursors increases the plateau capacity of hard carbon for sodium storage, Chemical Science 16 (1) (2025) 104–112.

[24] Y. Tao, S. Yan, Z. Ning, L. Jun-qing, T. Xiao-dong, W. Jin-ru, L. Hui, L. Zhan-jun, et al., Impact of pitch fraction oxidation on the structure and sodium storage properties of derived carbon materials, New Carbon Materials 40 (2) (2025) 409–421.

[25] H.-T. Zeng, W.-W. Kang, B.-L. Xing, G.-X. Huang, Q. Li, H. Hu, F.-L. Su, J.-B. Jia, C.-X. Zhang, Microstructure modulation of hard carbon derived from long-flame coal to improve electrochemical sodium storage performances, Fuel Processing Technology 267 (2025) 108159.

[26] J. Niu, J. Cheng, Z. Yi, C. Wang, X. Li, J. Chen, L. Xie, Y. Chang, X. Li, F. Su, et al., Promoting cross-linking reactivity of coal molecules via swelling strategy to realize high performance coal-derived hard carbon anode, Journal of Electroanalytical Chemistry 984 (2025) 119060.

Appendix: Techno-Economic Analysis

A process design and economic evaluation of the oxidant method to produce graphene oxide from Powder River Basin Coal Char was carried out, and a summary of the results is presented below.

Based on the laboratory work of Professor Johnson's research group, a preliminary process design has been developed to make a Graphene Oxide [GO] suitable for the reinforcement of Concrete from PRB Coal using a Modified Hummers Method. For 85,500 kTon/yr Graphene Oxide production rate, the CapEx was estimated at 131 MM$. The Netback Sales price [based on 15% return] was estimated to be 1$/lb GO. The GO Process feedstock is a finely ground [625 mesh] PRB Coal that has been Flash Pyrolyzed. The Pyrolysis Unit carries out the Pyrolysis step in the larger Coal Refinery Complex. Due to different grades of PRB Coal CHAR [pyrolysis product] produced by the Coal Refinery, the GO feedstock is stored in dedicated storage silos [F-920AB] in the Coal Refinery OSBL area. For a unit processing 20000 lb/hr dry, pulverized PRB coal CHAR, the CapEx was estimated at 131MM$. Table 1 summarizes the Production Cost statement. The economic calculations were done valuing GO at 0.5$/lb versus the current market price of around 1000$/lb. Also, no byproduct [purge] credit was taken for the dilute nitrogen fertilizer since the transportation costs will offset the Ag value.

PRODUCTION COST ESTIMATE REPORT

Production Cost Estimate Report

FILL IN BLUE CELLS	Evaluator	PKB		Date 11/27/2024			**NOTE: MM ==> million**	
	Product Name	GO		Location WY				
	Process Name	Modified Hummers to Make GO from PRB Coal CHAR						
	Nameplate Production	85,504	t/yr	(operating factor included)				
	ISBL (installed)	98	MM$					
	OSBL (installed)	33	MM$	Start-Up Costs	8.55	MM$		
	Total FCI (installed)	131	MM$	Working Capital	14.25	MM$		

Product and Revenue		Unit	Unit Price				Revenue MM$/yr	$/t of Product
GO Product (dry basis)		t	1000	$/t			85.50	1000
			0.500	*$/lb*				
Raw Materials		Unit	Unit Price		t	Consumption per Product	MM$/yr	$/t of Product
PRB Coal Char	(from CoalRefinery)	t	50	$/t	0.94	t/t product	4.00	47
				$/		/t product		
Gross Cost of Raw Materials							4.00	47
Byproducts	Price Basis Notes							
		t		$/t		t/t product	0.00	0
		MMBTU		$/MMBTU		MMBTU/t product	0.00	0
Total Byproduct Credits					0.0		0	0
Net Raw Materials (NRM)							4.00	47
Catalysts and Chemicals		unit		$/unit		unit/t product		
Nitric Acid [68wt%]		ton	400.00	$/ton	0.007	ton/t product	0.23	3
Lime (for pH neutralization)		ton	50.00	$/ton	0.003	ton/t product	0.01	0
Oxygen		ton	80.00	$/ton	0.093	ton/t product	0.64	7
Water (Purified)		ton	0.70	$/ton	0.638	ton/t product	0.04	0
Nitrogen Gas		ton	70.00	$/ton	0.100	ton/t product	0.60	7
Total Catalysts and Chemicals							1.52	18
Utilities								
Electricity	.75kW/HP	KWH	0.05	$/KWH	402	KWH/t product	1.72	20
Steam		MMBTU	5	$/MMBTU	22	MMBTU/t product	9.59	112
Cooling Water		MMBTU	0.6	$/MMBTU	21	MMBTU/t product	1.04	12
Total Utilities							12.35	144
Miscellaneous Variable Costs								
		unit		$/unit		unit/t product		
Disposal of Neutralized "ASH" Purge		ton	100	$/ton	0.040	ton/t product	0.35	4
Total Misc. Variable							0.35	4
Total Variable Costs (VC)							18.21	213

Fixed Costs			**Basis**					
Labor (basis: 8760 hr/yr * 1.6)	4.00	men/shift @	40.00	$/hr +	0.0	MM$/yr	2.24	26
Maintenance	4%	ISBL +	2%	OSBL +	0.0	MM$/yr	4.59	54
Lab	10%	Labor					0.22	3
Plant Overhead	10%	Labor + Maintenance + Lab					0.71	8
Taxes and Insurance	1%	FCI					1.31	15
Miscellaneous Fixed Costs					0.0	MM$/yr	0.00	0
Total Fixed Costs (FC)							9.08	106
Total Manufacturing Cost (TMC)							27.29	319
Margin (sales price - VC)							67.29	787

It is rather apparent that Utilities (Steam and Electricity) are the major Manufacturing Cost contributors. The Fixed Costs are the 2nd most significant portion. There is likely very little opportunity to significantly reduce the Fixed Cost contribution unless the GO production rate is significantly increased. Indeed, the Fixed Cost Maintenance contribution might be low due to the corrosivity of the Nitric Acid and the low price material of construction selected, 304L Stainless Steel. For Nitric Acid concentrations below 68%, 304L is a reasonable choice, provided halides are also not present. However, flow conditions and other chemistry that affect the passive layers may significantly increase corrosion issues. The Manufacturing Cost breakdown is shown below:

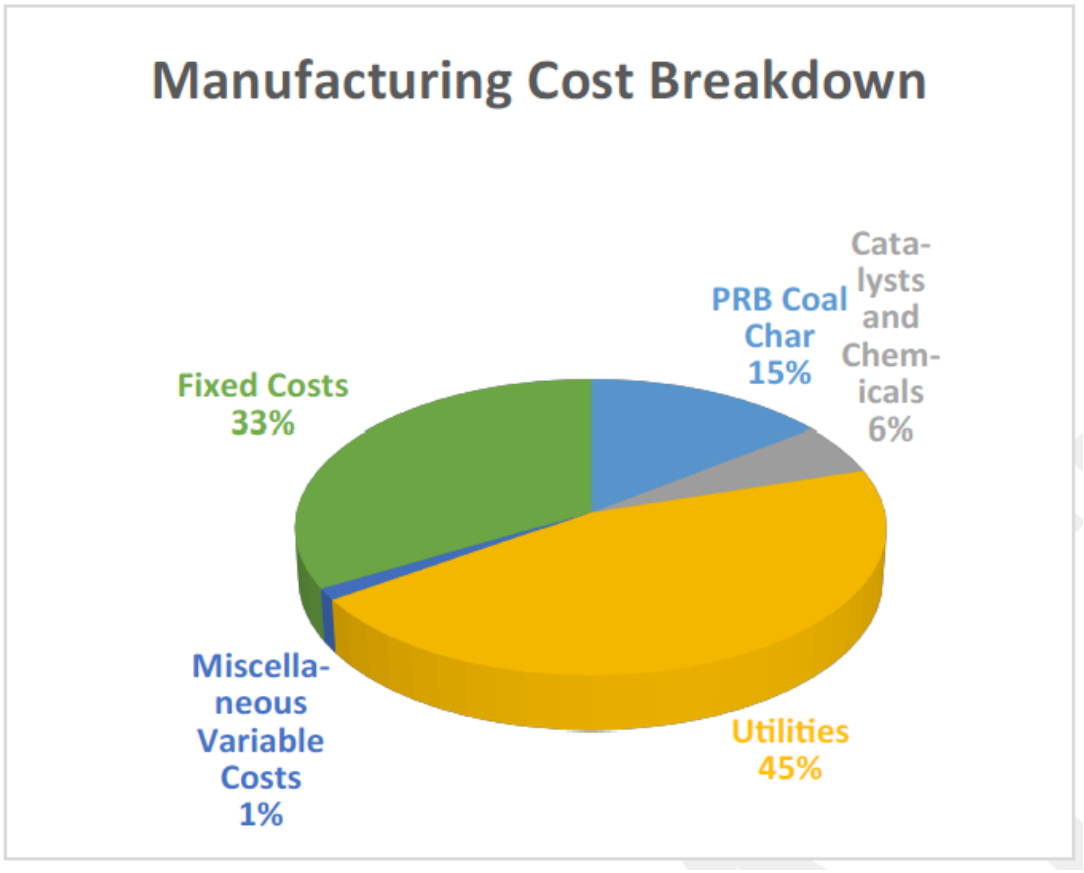

The present status of the design is preliminary. A variety of issues still need to be addressed as NO2 being converted back to Nitric Acid (and also avoid atmospheric emissions); the Solid-Liquid-Separation to recover the GO product from the reactor effluent; assumed 4-hour reaction time with Ultrasonics may need to be increased to 12 hours; corrosion testing in various steps will be required before scale-up; testing of the GO Product for reinforcement of Concrete must be completed to confirm the market size and pricing assumptions; conversion of the GO to Graphene should also be investigated,
and indeed, was the implicit assumption in the study several years ago when setting the production scale to 800 ton/year.

Summary of Economic Revitalization and Job Creation Outcomes

Coal-derived graphene materials for industrial applications

1. Apart from job creation, how will the project and/or the associated technology development and deployment support economic revitalization?

If the project is successful during the initial pilot phase, deployment of the technology on a commercial scale/in a commercial facility will not only create jobs but will also support economic development more broadly across Iowa and Wyoming. The state of Iowa participates in the Clean Jobs Midwest group. This consortium helps to advance the growth of the jobs in the renewable energy sector. Iowa job growth in manufacturing is robust, particularly with in clean energy technologies which the project would enhance. Wyoming has been the top net energy supplier in the United States for at least the last two decades. Many Wyoming communities have developed around and rely almost exclusively on the state's profuse stocks of crude oil, natural gas, and coal. While all Wyoming counties rely to some extent on revenue from mineral royalties, severance, and ad valorem taxes from fossil energy production, Campbell County is particularly dependent.[1] The mining industry accounts for the vast majority of state and local tax revenue generation in Campbell County. For instance, in a 2017 study conducted in part by the University of Wyoming on behalf of Campbell County, researchers found that mining accounted supported almost 9,000 jobs with labor earnings over $1 billion, representing over 20% of the county's total employment and over 40% of the county's total labor earnings.[2]

As conventional fossil fuel industries decline due to declining demand, the State of Wyoming and local Wyoming communities including but not limited to Campbell County have seen significant reductions in tax revenue. These reductions translate to reductions in public school and governmental funding, while lost opportunities for employment and population growth related to mining also affect the retail and service economies.

By developing alternative applications for Campbell County's immense coal resources, the Project will extend the economic viability of the region's existing coal facilities and potentially attract to the region other industries that require affordable sources of graphene or other carbon-based materials.

2. How many jobs could potentially be created by the project and/or associated technology development and deployment? As applicable, please quantify in terms of number of jobs created per unit of product, number of jobs created per unit of waste remediated, number of jobs created per unit of emissions mitigated, and/or another appropriate metric.

[1] A Campbell County Profile: Socioeconomics. (2017). Campbell County Board of County Commissioners. https://www.wyo-wcca.org/files/4015/0462/2986/Socioeconomic_profile__-_Campbell_County_March_2017.pdf. ("The Economic Research Service defines a county as mining dependent if 8 percent or more of total county employment is derived from Mining. Campbell County exceeds this threshold by nearly 3 times, indicating a very high dependency on Mining.").
[2] *Id.*

As this project is in its research and development phase, job creation will primarily be for research team members including three graduate students and two postdoctoral scholars. However, if the project is successful, it is likely to provide direct support for approximately five new jobs in Iowa (Story County) in new materials development and ten new jobs in Wyoming (Campbell County) related to pilot plant start up. As the technology is designed to extend the economic value of coal resources in the region, development and production of the technology could also sustain an unknown number of existing coal mining jobs. Corollary employment opportunities may arise in relation to the construction and engineering of facilities.

Construction of a coal conversion demonstration plant is underway in Campbell County, WY. 12 jobs associated with plant operation are expected.

Further battery related research has continued at Iowa State University – 2 graduate students. Integration of this material is proposed for an innovation fund project with ISU. The carbon material would be incorporated into the anode on solid state batteries. This could further employ and train researchers.

3. What will be the nature of the created jobs, including the extent to which they will include clean energy jobs?

The direct jobs created by a commercially viable operation will include positions in engineering, operations, manufacturing, and construction at a variety of skill levels. All jobs developed in the support of and as a result of the project will be clean energy jobs, to the extent that all efforts will be toward the development of alternative and renewable energies and identifying non-fuel uses of coal.

4. To what extent will the created jobs be at the prevailing wage?

All jobs created by the project will be at the prevailing wage and in alignment with skill and educational requirements. Since the jobs required will be at a variety of skill levels, the wages will reflect this. Jobs that require more education, training, and experience will offer wages competitive with other jobs with these requirements. Likewise for more entry level positions that require less education, training, and experience. With the facility requiring similar skill sets to the local mining industry, the prevailing wage of a mining industry employee would be a reasonable estimate. This was $129,000 inclusive of benefits in 2017 for Campbell County.

5. To what extent will the created jobs be located in power plant and coal communities that are economically distressed and/or have been harmed by the adverse environmental impacts of the energy industry?

Beyond the pilot phase, a significant portion of the jobs created in relation to a commercially viable operation will be in Campbell County, which has historically been an energy producing community with mining as its top industry. In the last decade, as demand for fossil energy resources has declined, so has employment in these industries. As such, many communities in Campbell County are particularly vulnerable to economic distress due to the energy transition and loss of jobs from fossil fuel industries.

In addition to the support to employment in these communities, the project will seek to provide lower emission operational solutions to the local energy industry, thereby working to mitigate further adverse environmental impacts to those communities.

6. What recruitment strategies will be used for: a) workers from the local community, and b) individuals who belong to groups that are historically underserved or underrepresented?

Recruitment of the necessary workforce to manage operations of a commercial facility will occur primarily in the local community. It will be important to employ, on a full-time basis, local residents to run the daily operations of the facility, so jobs will be advertised in local newspapers and online job posting sites. Recruiting of local businesses for construction and maintenance will also be important to take advantage of local expertise from the developed oil and gas workforce and to minimize transportation costs. The project may also utilize the existing recruitment and training networks of the surrounding community college districts to ensure that hiring efforts reach their diverse population of student candidates.

7. Will the skills possessed by the existing labor force be adequate for the created jobs, or will training be required for those workers?

The project will likely capitalize upon the skills and ability of the already-trained oil, gas, and mining workforce. The resident workforce consists of engineers educated in related fields of study as well as skilled technicians needed to operate a pilot plant, such as welders, electricians, and plant operators.